Dating exhumation and fault activity of the Lepontine Dome and Rhone-Simplon Fault regions through hydrothermal monazite-(Ce)

Christian A. Bergemann[1, 2], Edwin Gnos[2], Alfons Berger[3], Emilie Janots[4], and Martin J. Whitehouse[5]

[1]University of Geneva, Geneva, Switzerland
[2]Natural History Museum of Geneva, Switzerland
[3]University of Bern, Switzerland
[4]ISTerre University of Grenoble, France
[5]Swedish Museum of Natural History, Stockholm, Sweden

Correspondence: Christian Bergemann (christian.bergemann@unige.ch)

Abstract. Zoned hydrothermal monazite-(Ce) from fissures/clefts is used to gain new insights into the exhumation history of the Lepontine Dome in the Central Alps, and timing of deformation along the Rhone-Simplon Fault zone on the dome's western termination. These hydrothermal monazites-(Ce) directly date deformation and changes in physiochemical conditions through crystallization ages. 480 SIMS spot analyses from 20 individual crystals, including co-type material of the monazite-(Nd) type locality, record ages over a time interval of ∼19 and 2.7 Ma, with individual grains recording age ranges of 2 to 7.5 Myr. The combination of this age data with geometrical considerations and spatial distribution give a more precise young exhumation history for the area. In the north-east and south-west of the Lepontine Dome, units underwent monazite-(Ce) growth at 19-12.5 and 16.5-10.5 Ma respectively, followed by crystallization of monazite-(Ce) in the central part at 15-10 Ma. Fissure monazites-(Ce) are younger at the western limit of the dome with 13-7 Ma. A last age group around 8-5 Ma is limited to fissures/clefts associated with the Simplon normal fault and related strike-slip faults such as the Rhone Fault. The large data-set spread over significant metamorphic structures shows that the fissure mineral crystal-rock interaction, fluid flow and monazite-(Ce) stability are directly linked to the Lepontine Dome's evolution in space and time. A comparison between hydrothermal monazite-(Ce) thermo-chronometric data suggests that hydrothermal monazite-(Ce) dating could allow to identify areas of slow exhumation/cooling rates during ongoing tectonic activity.

1 Introduction

Metamorphic domes often experience a complex tectono-metamorphic evolution (*e.g.* Schmid *et al.*, 2004; Steck *et al.*, 2013). For the Lepontine Dome of the European Alps, this evolution is an interplay between exhumation and deformation during doming and motion along large fault systems that dominate the western regions of the dome. Although much of the retrograde orogenic evolution of the area is well known, hydrothermal monazite-(Ce) ages complement existing cooling ages of thermo-chronometers by providing crystallization and dissolution-precipitation ages that directly date low-T tectonic activity.

Monazite, (LREE,Th,U)PO_4, is considered an excellent mineral for the dating of geologic processes (*e.g.* Parrish, 1990). It is highly resistant to radiation damage (*e.g.* Meldrum *et al.*, 1998, 1999, 2000) and shows negligible Pb loss by diffusion

(Cherniak *et al.*, 2004; Cherniak and Pyle, 2008). Nonetheless, monazite remains reactive after crystallization, as it can experience dissolution-recrystallization facilitated through hydrous fluids (*e.g.* Seydoux-Guillaume *et al.*, 2012; Janots *et al.*, 2012; Grand′Homme *et al.*, 2016).

Fissures and clefts occasionally contain hydrothermal monazite-(Ce). They represent voids partially filled by crystals that precipitated on the fissure walls from hydrous fluids during late stage metamorphism (Mullis *et al.*, 1994; Mullis, 1996). Dating such mineralization is often difficult due to later overprinting along with multiple stages of fluid activity (Purdy and Stalder, 1973). Fissures and clefts in some metasediments and metagranitoids have long been known to contain well-developed monazite-(Ce) crystals (Niggli *et al.*, 1940), but it is only recently that some of these were dated (*e.g.* Gasquet *et al.*, 2010; Janots *et al.*, 2012). Although other minerals like micas and adularia are common in alpine fissures, they are often affected by overpressure/excess argon, (*e.g.*, Purdy and Stalder, 1973), and it is not always clear if these ages represent crystallization or cooling (*e.g.*, Rauchenstein-Martinek, 2014). The fissures and clefts in the Lepontine region formed after the metamorphic peak, in relation to extensional tectonic activity. Accordingly, fissures and clefts are oriented roughly perpendicular to the lineation and foliation of the host rock. The fluid that intruded during fissure formation (300-500°C; Mullis *et al.*, 1994; Mullis, 1996) interacted with the wall rock. This triggered dissolution and precipitation of minerals in both host rock and fissure, leading to the formation of a porous alteration halo in the surrounding wall rock. Complex growth domains are common in hydrothermal monazite-(Ce) from such fissures showing both, dissolution and secondary growth (*e.g.* Janots *et al.*, 2012; Bergemann *et al.*, 2017, 2018), as well as dissolution-reprecipitation reactions resulting in patchy grains (*e.g.* Gnos *et al.*, 2015). In contrast to metamorphic rocks, where monazite-(Ce) rarely exceeds 100μm, fissure monazite-(Ce) is commonly mm-sized, with large individual growth domains. This permits dating individual domains precisely by using secondary ion mass spectrometry (SIMS), resolve growth duration and identify phases and single events of tectonic activity (*e.g.* Janots *et al.*, 2012; Berger *et al.*, 2013; Bergemann *et al.*, 2017, 2018, 2019).

The aim of this study is to illustrate that hydrothermal monazite-(Ce) dating provides information about the tectonic evolution of the Lepontine Dome.

2 Geological setting

2.1 Evolution of the study area

The formation of the nappe stack of the European Alps caused by the collision of the European and Adriatic plates was followed by the development of several metamorphic areas (Tauern, Rechnitz in the Eastern Alps, and Lepontine in the Central Alps; *e.g.* Schmid *et al.*, 2004). Their formation was related to crustal shortening associated with coeval orogen-parallel extension (*e.g.* Mancktelow, 1992; Ratschbacher *et al.*, 1989; Ratschbacher *et al.*, 1991). The Western and Central Alps with the Lepontine Dome have consequently had a complex tectonic and metamorphic history.

Early high-pressure metamorphism in the Western Alpine Sesia-Lanzo Zone during subduction below the Southern Alps is dated at 75-65 Ma (*e.g.* Ruffet *et al.*, 1997; Rubatto *et al.*, 1998; Regis *et al.*, 2014). This was followed by underthrusting and nappe stacking from *ca.* 42 Ma on during continental collision linked with a transition from high-P/low-T to barrow type

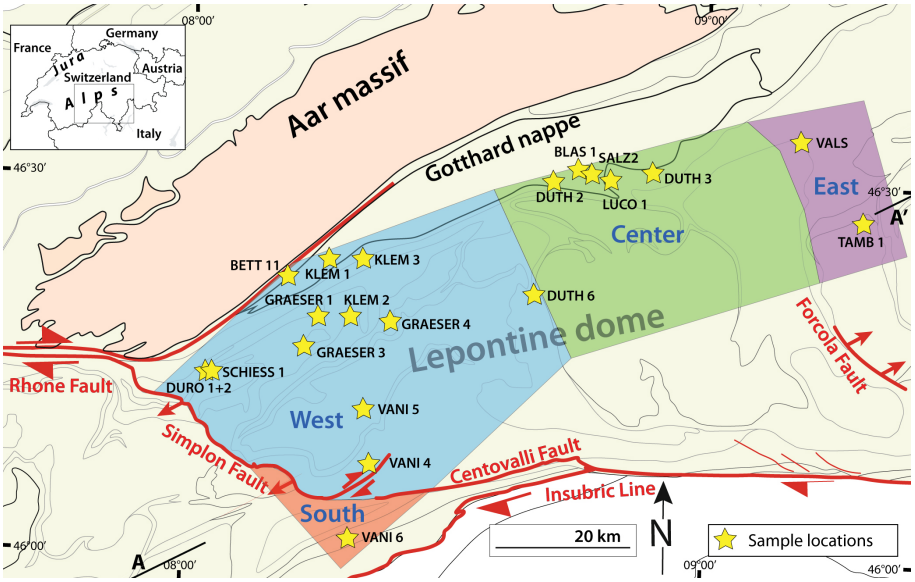

Figure 1. Map of the Lepontine Dome, modified from Steck *et al.* (2013) and Schmid *et al.* (2004). Colored areas mark the areal division in the context of this study.

metamorphism (medium P/T; *e.g.* Köppel and Grünenfelder, 1975; Markley *et al.*, 1998; Herwartz *et al.*, 2011; Boston *et al.*, 2017). Peak metamorphic conditions in the Lepontine area (in excess of 650°C in some regions) were reached diachronously from south to north around 30-19 Ma (*e.g.* Schärer *et al.*, 1996). Barrovian metamorphism was followed by exhumation starting in the east and migrating to the west of the Lepontine Dome, with vertical displacement along the Insubric Line starting as early as 30 Ma (*e.g.* Hurford, 1986; Steck and Hunziker, 1994). Accelerated cooling below 500°C first occurred at ∼26 Ma in the central Lepontine Dome (Hurford, 1986). This was followed in the eastern Lepontine Dome and along the Insubric Line between 22 and 17 Ma by a period of rapid cooling (Steck and Hunziker, 1994; Rubatto *et al.*, 2009) after which exhumation slowed down. The area to the west in the surrounding of the Rhone-Simplon Line experienced phases of accelerated cooling somewhat later at 18-15 Ma and 12-10 Ma (Campani *et al.*, 2014).

The western and southwestern limits of the study area are dominated by the Rhone-Simplon Fault system, its extensions to the Rhine-Rhone Line to the north along the Aar Massif and the Centovalli Fault to the south (Fig. 1). The extensional Simplon Fault zone (SFZ) was active contemporaneous with thrusting in the external Alpine domain (*e.g.*, Grosjean *et al.*, 2004). The ductile-brittle transition of the SFZ was constrained to the time between 14.5 and 10 Ma (Campani *et al.*, 2010). Brittle deformation of the SFZ and Centovalli Fault continued after this (Zwingmann and Mancktelow, 2004; Surace *et al.*, 2011), with the youngest displacement activity dated to *ca.* 5-3 Ma (Campani *et al.*, 2010).

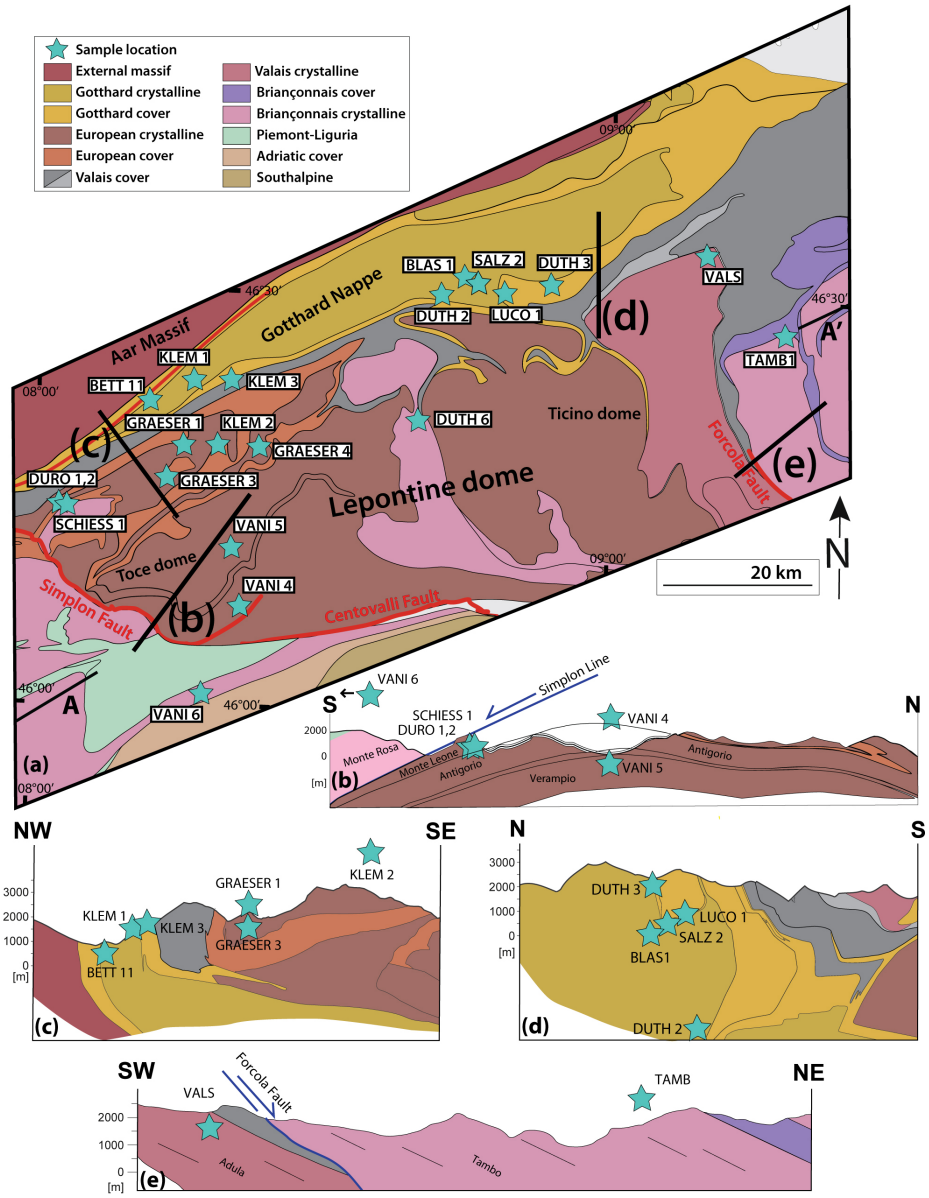

Figure 2. Tectonic overview over the study area. (a) Tectonic sketch map modified after Schmid *et al.* (2004) and Steck *et al.* (2013), sample BLAU is from Janots *et al.* (2012); (b) Tectonic section over the Simplon Fault zone into the western Lepontine, based on Campani *et al.* (2014); (c) Tectonic section through the western Northern Steep Belt, modified and extended after Leu (1986); (d) Tectonic section through the eastern Northern Steep Belt, redrawn after Wiederkehr *et al.* (2008); (e) Tectonic section across the Forcola normal fault, see also Meyre *et al.*, (1998) and Berger *et al.* (2005). Profiles (b)-(e) are not to scale with map (a).

Table 1. Information on sample localities for all analyzed grains. Sample GRAESER 1 has identification number NMBa 10226, VALS has NMBE43124.

Region	Sample	Locality	Latitude	Longitude	Altitude (m)
South	VANI 6	Cava Maddalena, Beura	46°04.30’	8°17.71’	260
West	BETT 11	Bettelbach, Niederwald, Goms	46°25.62’	8°11.70’	1460
	DURO1	Doru, Gantertal, Simplon	46°17.63’	8°02.07’	1160
	DURO2 Simplon	Doru, Gantertal,	46°17.64’	8°02.07’	1160
	DUTH 6 di Prato (Lavizzara)	Pizzo Rüscada, Valle	46°24.57’	8°40.09’	2420
	GRAESER 1	Lärcheltini, Binntal	46°22.3’	8°14.9’	1860
	GRAESER 3	Wannigletscher, Cherbadung, Binntal	46°19.5’	8°23.4’	2560
	GRAESER 4	Monte Giove, Val Formazza	46°21.9’	8°13.0’	2720
	KLEM 1 Blinnental	Grosses Arsch,	46°26.71’	8°16.33’	1900
	KLEM 2	Alpe Devero, Val Antigorio	46°22.16’	8°18.44’	2340
	KLEM 3	Griessgletscher	46°26.59’	8°19.46’	2840
	SCHIESS 1	Schiessbach/Simplon	46°18.13’	8°04.18’	1760
	VANI 4	Montecrstese	46°09.60’	8°19.18’	370
	VANI 5	Crino Baceno	46°15.13’	8°19.14’	710
Center	BLAS 1	Piz Blas, Val Nalps, Sedrun	46°34.68’	8°43.98’	2790
	DUTH 2	Lago Sucro, Val Cadlimo	46°33.80’	8°41.50’	2620
	DUTH 3	Lago Retica, Lagi di Campo Blenio	46°34.45’	8°53.57’	2400
	LUCO 1	Lucomagno	46°33.79’	8°48.10’	1915
	SALZ 2	Piz Scai	46°34.5’	8°45.8’	2740
East	TAMB 1	Pizzo Tambo, Splügen	46°30.48’	9°18.35’	2460
	VALS	Vals, Valsertal	46°37.3’	9°17.3’	3150

2.2 The study area

The study area comprises the part of the Lepontine Dome in which mineralized fissures/clefts are commonly found (Fig. 1), from the Tambo nappe, east of the Forcola Fault, over the central Lepontine Dome to the Simplon Fault in the west/southwest south of the Centovalli Fault, and the southern Gotthard nappe to the north (see Fig. 2 for the tectonic position of the samples). The 20 monazite-(Ce) samples dated in this study were divided into four groups (Fig. 1). These are (1) the area to the west of the Adula nappe (East; 2 samples), (2) the Lepontine Dome east of the Verzasca anticline including part of the southern Gotthard nappe (Center; 5 samples), (3) the west equally bound by the Verzasca anticline, the Rhone-Simplon Fault to the west and adjacant south-western Gotthard nappe (West; 12 samples), and (4) the area to the south of the Centovalli and southern Simplon Faults (South; 1 sample).

3 Study approach and techniques

3.1 Monazite-(Ce) crystallization and alteration under hydrothermal conditions

The possibility of hydrothermal monazite-(Ce) crystallization within an open fissure/cleft depends on the chemical composition of the aqueous fluid filling it. Following the initial formation of a fissure/cleft, the intruding metamorphic fluid (300-500°C; Mullis *et al.*, 1994; Mullis, 1996) leaches and partly dissolves the surrounding host rock, and leads to crystallization of mineral phases on the fissure/cleft wall under chemical equilibrium conditions. If the resulting chemical equilibrium between fluid phase, cleft minerals and those parts of the wall rock accessible to the fluid is disturbed, a new cycle of dissolution and crystallization within the cleft occurs. Chemical disequilibration is generally triggered by tectonic activity causing a deformation of the fissure/cleft and results in sudden changes in the P-T conditions, the influx of a new fluid, or the exposure of previously unaltered wall rock (*e.g.* Mullis *et al.*, 1994; Rolland *et al.*, 2003; Sharp *et al.*, 2005). Since the fissure/cleft remains fluid filled, these mechanisms of (partial) dissolution and precipitation of newly formed cleft minerals occurs repeatedly, resulting in the strong zonation, alteration and dissolution features of most cleft minerals (*e.g.* Mullis, 1996; Sharp *et al.*, 2005; Heijboer, 2006). Therefore the mineral association of a cleft is the result of a series of equilibrium states and does not represent a mineral paragenesis. This means that each crystal or crystal part was during its formation in chemical equilibrium with the surrounding fluid, so that each primary chemical zone within a crystal represents a change in the cleft fluid chemical composition.

Hydrothermal monazite-(Ce) typically crystallizes at temperatures below ∼350°C/∼300°C (Gnos *et al.*, 2015; Bergemann *et al.*, 2017, 2018). Due to the presence of fluid in the cleft, it continues to be reactive down to 200°C or somewhat below (*e.g.* Townsend *et al.*, 2000; Bergemann *et al.*, 2018). During the formation of a grain, any tectonic activity that changes the chemical equilibrium within a cleft, causes the crystal to develop a primary chemical zonation usually visible in BSE images. After crystallization, monazite-(Ce) shows practically no U-Th-Pb diffusion at the prevalent P-T conditions (Cherniak and Pyle, 2008). However, the changing chemical conditions in a hydrothermal environment may not only cause new growth around an existing grain, but can result in partial (re-)crystallization/dissolution-reprecipitation in equilibrium with the cleft fluid (*e.g.* Janots et al, 2012; Bergemann *et al.*, 2017; Grand′Homme *et al.*, 2018). The dissolution-reprecipitation processes

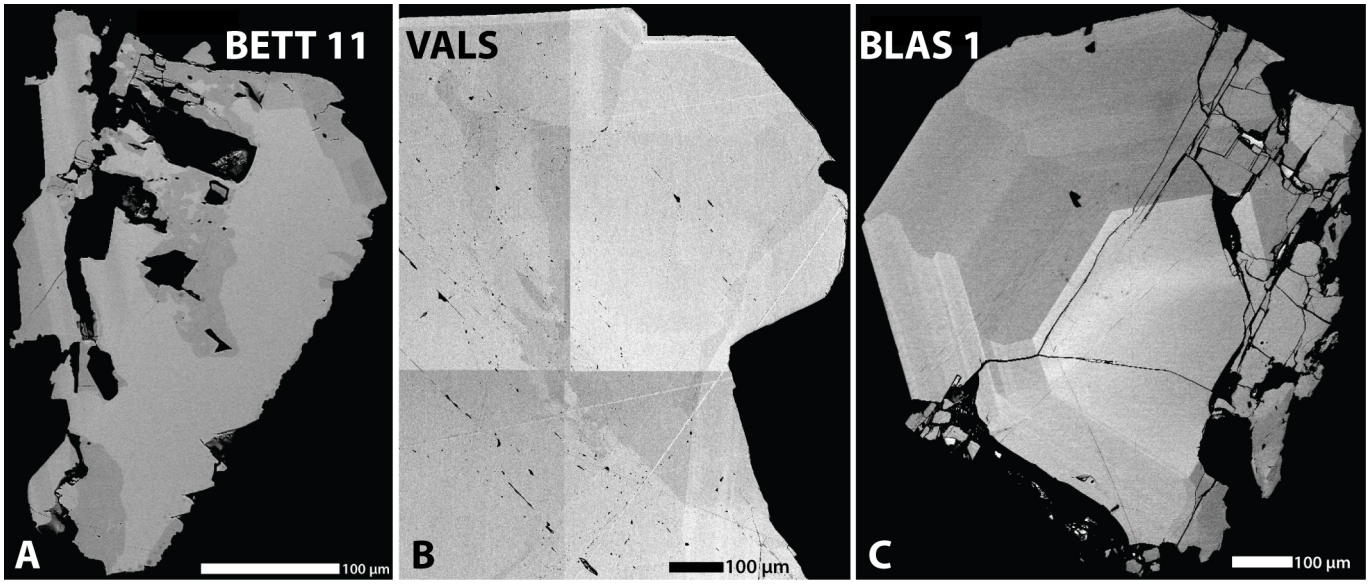

Figure 3. BSE image of monazite-(Ce) samples showing different kinds of internal primary and alteration structures. (A) The dark grain areas of the grain, primarily located close to rims and inclusions, display sharp irregularly shaped borders and porosity. These areas consist of secondary monazite that is *ca.* 2.5 Myr younger than the pristine lighter grain parts (Fig. 5b). Image (B) shows part of a large grain with partially preserved sector-like zonation. Indications for alteration are irregularly shaped secondary zonation, both patchy in the middle and wavy on the right side, as well as porosity and fractures. The light rim visible at the top likely represents a late overgrowth but yields some of the oldest ages of the grain, predating those of some of the interior grain parts by several million years (Fig. 5t). The grain in (C) displays multiple rims combined with sector-like zonation around a central part. Although the grain shows practically no alteration features, the outer rim has the oldest and most homogeneous age pattern, with the central part possessing a wider age range with some significantly younger ages (Fig. 5m, Supplement Table 1). The youngest ages were found in part of the inner rim, postdating all other ages measured in the second rim or center by several million years.

may be initiated on any part of the crystal in contact with the surrounding fluid. A self-sustaining reaction front propagates in this case into the mineral for as long as the interfacial fluid remains connected to a fluid reservoir (*e.g.* Putnis, 2002, 2009). The alteration is therefore not limited to grain rims, but commonly occurs along mineral inclusion interfaces, cracks and microcracks due to which also internal parts of a crystal may be altered (Fig. 3a, b; Grand′Homme *et al.*, 2018). These processes may be active as long as conditions in the cleft stay within the monazite-(Ce) formation temperature window and stability field, and appear to be largely temperature independent with only slightly increasing reaction speeds with increasing temperature (Budzyn *et al.*, 2011). Therefore, several (re-)crystallization or dissolution-precipitation cycles may occur over the active lifespan of a monazite-(Ce) crystal (*e.g.* Bergemann *et al.*, 2018, 2019). Later reactions may be aided by porosity and fractures in the primary and secondary monazite-(Ce), induced by the previous dissolution-reprecipitation/recrystallization events, by bringing an increased crystal volume into direct contact with the fluid (Putnis, 2002, 2009). Possible signs of these alteration processes recognizable in BSE images are irregularly shaped (Fig. 3 a, b) or weak (Fig. 3 b) internal zonation, or

cross-cutting by secondary zones (Fig. 5 j, k), as well as a high porosity (Fig. 3 a, b; *e.g.* Gnos *et al.*, 2015; Bergemann *et al.*, 2017, 2018). Micro-scale alteration along cracks, inclusions and porosity may produce altered areas within a crystal that cannot be recognized in BSE images but yield a different age (Fig. 3c; Grand′Homme *et al.*, 2018). Dissolution-precipitation processes may sometimes largely preserve the chemical composition of an affected crystal part, possibly due to only small pore fluid volumes involved in the reaction that did not equilibrate completely with the fluid surrounding the crystal, consequently areas affected by alteration that posses different chemical compositions may have reprecipitated simultaneously (Grand′Homme *et al.*, 2016; Bergemann *et al.*, 2017, 2018).

3.2 Analytical techniques

Most of the samples were provided by mineral collectors, as hydrothermal cleft monazite-(Ce) is uncommon and often difficult to detect in the field when covered by dirt or chlorite. See Table 1 for location details. Monazites-(Ce) were individually polished to the level of a central cross section and assembled in mounts of several grains. Backscatter electron (BSE) images were then obtained, using a Zeiss DSM940A electron microscope at the university of Geneva and a beam current of 3.5 nA. As the surface of the mounts has to remain flat for ion probe dating, element mapping that would cause damage to the epoxy is not possible. Secondary ion mass spectrometry (SIMS) spot analyses (Fig. 5) were placed according to visible domains in these images. As far as possible, spot measurements next to cracks were avoided, as the Th-Pb isotope measurements may be disturbed in such areas due to unevenness in the sample surface (Janots *et al.*, 2012; Berger *et al.*, 2013).

Th-Pb analyses were conducted at the Swedish Museum of Natural History (Nordsim facility) on a CAMECA ims1280 SIMS instrument. Analytical methods and correction procedures followed those described by Harrison *et al.* (1995), Kirkland *et al.* (2009), and Janots *et al.* (2012), using a -13 kV O^{2-} primary beam of *ca.* 6 nA and nominal 15μm diameter. The mass spectrometer was operated at +10kV and a mass resolution of *ca.* 4300 (M/ΔM, at 10% peak height), with data collected in peak hopping mode using an ion-counting electron multiplier. Unknowns were calibrated against monazite-(Ce) standard 44069 (Aleinikoff *et al.*, 2006). Lead isotope signals were corrected for common Pb contribution using measured ^{204}Pb and an assumed present-day Pb isotope composition according to the model of Stacey and Kramers (1975). The measurement of ^{204}Pb is subject to an unresolvable molecular interference by $^{232}Th^{143}Nd^{16}O_2^{++}$, also affecting ^{206}Pb and ^{207}Pb to a lesser degree through replacement of ^{16}O by heavier O-isotopes, which may result in an overestimation of common Pb concentrations. A correction was applied whenever the $^{232}Th^{143}Nd^{16}O_2^{++}$ signal at mass 203.5 exceeded the average background signal on the ion-counting detector by three times its standard deviation. Age calculations use the decay constants recommended by Steiger and Jäger (1977). The Th-Pb ages were corrected for common Pb and doubly charged $^{232}Th^{143}Nd^{16}O_2^{++}$ overlap and are reported at 2σ uncertainties. Weighted mean age plots were done using Isoplot v. 3.75 (Ludwig, 2012).

4 Th-Pb monazite-(Ce) dating

The dating of hydrothermal monazite-(Ce) differs from thermo-chronometers that posses a closure temperature insofar, as a crystal may record several ages due to new crystallization or alteration of crystal parts. The grains directly record tectonic

Table 2. Overview list of the ^{232}Th-^{208}Pb age range and significant minimum and maximum ages obtained for each grain, and weighted mean domain ages that could be calculated for the samples.

Region	Sample	Figure	# of analyses	Spot age range of sample (Ma)	min. age (Ma)	max. age (Ma)	Weighted mean domain ages (Ma)	MSWD	# of points
South	VANI 6	5a	24	16.80 ± 0.31 – 10.62 ± 0.18	16.80 ± 0.31	10.62 ± 0.18	14.68 ± 0.47	2.8	5
West	BETT 11	5b	19	10.55 ± 0.33 – 7.34 ± 0.26	10.31 ± 0.31	like mean age	9.85 ± 0.29	2.1	12
							7.53 ± 0.31	0.53	3
	DURO 1	5c	25	10.82 ± 0.26 – 8.21 ± 0.20	10.82 ± 0.26	like mean age	9.95 ± 0.18	0.37	7
							9.50 ± 0.23	0.65	4
							8.34 ± 0.20	0.29	4
	DURO 2	5d	32	11.48 ± 0.28 – 7.02 ± 0.18	11.48 ± 0.28	like mean age	7.63 ± 0.13	0.55	8
							7.18 ± 0.18	0.50	4
	DUTH 6	5e	26	12.60 ± 0.37 – 9.33 ± 0.32	12.60 ± 0.37	like mean age	11.90 ± 0.27	1.5	12
							9.74 ± 0.22	1.5	13
	GRAESER 1	5f	31	12.14 ± 0.30 – 7.57 ± 0.19	12.14 ± 0.30	like mean age	9.16 ± 0.24	0.19	4
							8.78 ± 0.27	1.8	7
							7.73 ± 0.16	0.54	6
	GRAESER 3	5g	17	15.60 ± 0.61 – 6.36 ± 0.39	15.60 ± 0.61	6.36 ± 0.39			
	GRAESER 4	Appendix	2	12.25 ± 0.51 – 11.88 ± 0.47	12.25 ± 0.51	11.88 ± 0.47			
	KLEM 1	5h	24	10.64 ± 0.26 – 7.97 ± 0.20	10.64 ± 0.26	7.97 ± 0.20	8.43 ± 0.20	0.94	5
	KLEM 2	5i	17	13.65 ± 0.33 – 9.47 ± 0.40	like mean age	like mean age	13.44 ± 0.31	0.57	5
							11.74 ± 0.32	0.83	5
							10.12 ± 0.94	2.6	4
	KLEM 3	5j	24	12.96 ± 0.46 – 8.43 ± 0.32	like mean age	8.43 ± 0.32	12.50 ± 0.34	0.65	6
							11.99 ± 0.66	2.3	6
							10.17 ± 0.52	2.4	7
	SCHIESS 1	5k	27	9.94 ± 0.25 – 6.78 ± 0.18	6.90± 0.18	like mean age	9.78 ± 0.22	0.41	5
							7.03 ± 0.38	2.3	5
	VANI 4	5l	16	9.27 ± 0.43 – 6.89 ± 0.37	9.27 ± 0.43	6.89 ± 0.37	8.03 ± 0.44	2.2	7
	VANI 5	5m	20	8.07 ± 0.36 – 2.69 ± 0.11	7.45 ± 0.22	2.69 ± 0.11	7.21 ± 0.43	1.9	6
							5.53 ± 0.60	3.5	5
Center	BLAS 1	5n	18	14.49 ± 0.26 – 7.82 ± 0.22	14.49 ± 0.26	7.82 ± 0.22	12.83 ± 0.39	2.0	5
	DUTH 2	5o	16	14.34 ± 0.41 – 11.15 ± 0.43	14.34 ± 0.41	11.15 ± 0.43	13.41 ± 0.70	2.0	5
	DUTH 3	5p	26	14.53 ± 0.43 – 10.61 ± 0.34	14.53 ± 0.43	0.61 ± 0.34	13.48 ± 0.53	1.8	7
	LUCO 1	5q	25	14.74 ± 0.30 – 9.90 ± 0.17	14.74 ± 0.30	9.90 ± 0.17	14.23 ± 0.23	0.77	5
	SALZ 2	5r	28	14.28 ± 0.74 – 10.51 ± 0.39	14.28 ± 0.74	like mean age	12.98 ± 0.25	2.2	17
							10.95 ± 0.37	1.5	9
East	TAMB 1	5s	24	19.02 ± 0.47 – 8.32 ± 0.11	19.02 ± 0.47	8.32 ± 0.11	17.49 ± 0.40	0.72	4
							14.3 ± 1.1	2.7	4
							13.28 ± 0.98	3.0	5
	VALS	5t	43	16.43 ± 0.61 – 12.09 ± 0.57	16.43 ± 0.61	like mean age	15.27 ± 0.35	1.1	7
							14.70 ± 0.41	0.81	6
							12.61 ± 0.36	0.57	7

activity instead of cooling through new/re-crystallization, as *e.g.* in the case of Ar-Ar dating in white micas. Consequently, unless coupled with fluid inclusion analysis, a hydrothermal monazite-(Ce) age in itself only provides a very general idea of temperature conditions (*ca.* 350-200°C or somewhat below; Gnos *et al.*, 2015; Bergemann *et al.*, 2017, 2018) and more information on temperatures needs to come from a comparison with thermo(-chrono)meters.

The SIMS spot analyses were distributed on the basis of domains visible in BSE images, among these the center and outer rim if distinguishable,to capture the crystallization duration. In order to obtain more robust growth domain ages, the selected domains were large enough to place a minimum of three measurement spots. The number of domains dated was limited by available machine time. Only ^{208}Pb/^{232}Th ages were used, as the Th-Pb system is favorable in dating hydrothermal monazite-(Ce) due to high Th/U ratios at low U content, which preclude the use of the ^{207}Pb/^{235}U system. Additionally, the high Th/U ratios and young age oft the samples also exacerbate the uncorrectable excess in ^{206}Pb due to the incorporation of ^{232}Th, an intermediate decay product of ^{238}U (Janots *et al.*, 2012). This means that only ^{208}Pb/^{232}Th single or weighted mean ages instead of concordia ages should be used.

Previous studies found no simple chemical criteria to identify altered zones and have shown that U-Th-Pb contents seem to be the easiest way to differentiate between zones, both primary and secondary (*e.g.* Gnos *et al.*, 2015; Bergemann *et al.*, 2017). Figure 5 includes plots showing compositional varation used as a basis for domain age calculations. The derived spot ages were grouped together on the basis of chemical composition representing crystal formation or replacement under changing equilibrium chemical conditions, and, if possible, spatial distribution across the sample according to zonation visible on BSE images. Whenever age clusters were found on the basis of these groups, weighted mean domain ages were calculated (Fig. 5), as these could be shown to date tectonic activity (Grand′Homme *et al.*, 2016; Bergemann *et al.*, 2017, 2018, 2019; Ricchi *et al.*, 2019). Since any new crystallization or alteration associated with a change in chemical composition must have happened in equilibrium with the surrounding fluid, any age cluster within a chemical group must be due to those crystal parts' simultaneous formation or alteration. Therefore, two chemically distinct groups that yield, within error, identical weighted mean ages, still signify two distinct crystal formation/alteration events closely following each other. In areas that experienced strong and discrete tectonic events, usually in the vicinity of shear zones, this approach allows the calculation of domain ages for a majority of the analyzed spots from the dataset of a sample (*e.g.* Janots *et al.*, 2012; Berger *et al.*, 2013; Bergemann *et al.*, 2017, 2019; Ricchi *et al.*, 2019). Although, as only a limited number of analyses are possible to be obtained for each grain, some of the weighted mean ages may only combine a small number of individual ages. This appears to be especially true for ages dating late stage events (*e.g.* Berger *et al.*, 2013; Grand′Homme *et al.*, 2016; Bergemann *et al.*, 2017, 2018).

A problem in this approach, used in other areas of the Alps, is that large parts of the Lepontine Dome region experienced more than two distinct deformation events and/or phases of prolonged small scale tectonic activity, likely during exhumation. Experiments have shown that a reason for a large age scatter in crystal domains affected by alteration may be an incomplete age resetting due to the survival of primary monazite nanoscale domains (Grand′Homme *et al.*, 2018). This may have caused the observed spread out age patterns without age clusters in zones visible in BSE, which impede the calculation of weighted mean ages (Fig. 5). Especially prolonged phases of low-intensity tectonic activity would presumably repeatedly cause small volumes of monazite-(Ce) to reprecipitate during re-equilibration of the fluid chemistry.

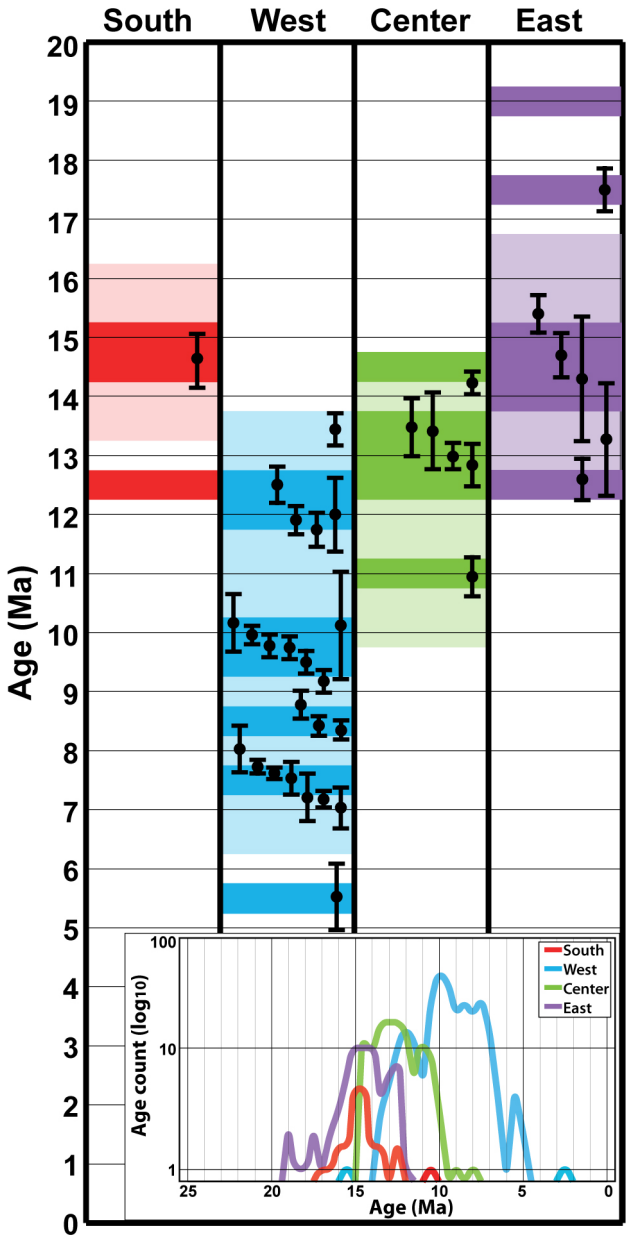

Figure 4. Time diagram combining identified peaks from the inset and weighted mean ages of all samples from the Lepontine Dome. The inset shows an age probability density plot representing the dataset of each region (Fig. 1) according to the number of ages per 0.5 Myr interval. In the time diagram, darker colors represent peaks or plateaus from the inset indicating times of intense monazite formation/alteration. Lighter shades mark the remaining times for which more than one age was recorded, indicating either only limited tectonic activity or mixing ages. Black error bars indicate weighted mean ages from this study.

Additionally, as stated above, altered areas may preserve their overall chemical composition but consist of a submicroscopic mix of different phases (*e.g.* Grand′Homme *et al.*, 2016), and analyses belonging to the same chemical group may therefore show a large age scatter. The limited number of analyses per grain would therefore result in many individual ages being discarded for these areas. Accordingly, events may, especially in larger grains, not be recognized if looking at the well defined weighted mean ages only. To avoid this, the entire dataset of each region was plotted according to the number of ages per 0.5 Myr interval to identify age clusters across the grains of a given region (Fig. 4 inset). The identified age peaks and phases for which a significant number of ages were obtained were then combined with the weighted average ages to visualize distinct events or phases of tectonic activity (Fig. 4). Age peaks of a region's dataset and weighted mean ages of individual grains generally agree, with some phases of age recording visible in the overall age record not identified through weighted mean ages. For the interpretation of the data, weighted mean ages are preferable to pinpoint deformation events. However, at least the beginning and end of the age record within a sample must have a geological significance since their recording must have been triggered by tectonic activity, even if one assumes all ages in between to be simply mixing ages. Accordingly, weighted mean ages are in the following generally discussed as precise ages, while spot ages are treated as approximate ages.

4.1 Results

The ion-probe measurement data set is given in the data Appendix Table A1 and can be found in the PANGAEA data base (https://doi.org/10.1594/PANGAEA.898689). The age data of the individual samples and the whole data set cover a large range of *ca.* 16 Myr, covering the time between ∼19 and 2.7 Ma. Individual grains record ages over a lifetime of 2 to 7.5 Myr. An overview over the individual age ranges and the weighted mean domain ages that could be calculated for the individual samples is shown in Table 2. Figure 5 shows the measurement positions, weighted mean domain ages, where available, a graphical representation of the measured ages and a chemical for each sample the best shows the different groups.

Sample GRAESER 4 (Appendix Fig. A1; Appendix Table A1) is a grain (co-type) from the monazite-(Nd) type locality (Graeser and Schwander, 1987). Due to very low Th contents only two spots yielded ages of 11.88 ± 0.47 and 12.25 ± 0.51 Ma, clearly indicating that the monazite-(Nd) crystallized coevally with monazite-(Ce).

Typical for hydrothermal cleft/fissure monazite, the contents of Th and U are generally relatively low compared to monazite from other geological environments (Appendix Table A1; Janots *et al.*, 2012). With Th contents generally ranging between 5000 and 60000 ppm, with (parts) individual samples considerably lower (down to 1000 ppm) or higher (up to 110000 ppm), while U contents are below 1000 ppm (only KLEM 3 up to 3300 ppm), resulting in high Th/U ratios of up to several hundred. Lead contents show a spread from a few up to several hundred ppm, with common Pb contents generally considerably below 10%. However, a number of measurements in GRAESER 3 and TAMB 1 show very high common Pb contents above 70% with a maximum of 99%. With the exception of sample BLAS 1, all sample grains show at the least some alteration features (irregular, wavy or unclear zonation, porosity) and can roughly be divided into five partly overlapping groups on the basis of their appearance in BSE images (Fig. 5): (1) Sector like zonation:

DUTH 6 shows some signs of alteration and complex zonation in the inner part of the grain.

GRAESER 3 shows no clear signs of alteration, but an extreme zonation in both Th (∼1800-113000 ppm) and U (∼10-680 ppm) contents according to visible zonation and elevated (>10%) to extreme (65-99%) common Pb contents. The ages derived from the low Th measurements should be treated with caution, as they show a greater spread at higher error than the other measurements.

VANI 4 shows in places strong signs of alteration.

VANI 5 displays in places only weak zonation with sometimes strong alteration signs. Thorium contents are relatively low at 1600-10800 ppm, and common Pb contents elevated but mostly below 20%.

VALS, by far the largest analyzed grain, that shows in places only weak zonation with sometimes strong alteration features. Thorium contents are low (>3500 ppm) with only an overgrowth rim showing higher contents (up to 12300 ppm). Common Pb contents are elevated but remain below 25%.

(2) Sector like + oscillatory/ring zonation:

BLAS 1 shows no visible signs of alteration, but the interior part of the crystal gives younger ages than the outer part.

DURO 1 has strong zonation with only minor signs of alteration.

KLEM 1 shows signs of alteration, and the zonation is diffuse in places like the center and part of the rim.

SCHIESS 1 shows in parts strong alteration signs and the primary zonation is cut in places.

(3) Clear distinction between primary and altered zones:

BETT 11 is the only sample that is featureless, but it shows altered areas around holes and along rims.

VANI 6 displays oscillatory-complex zonation, with clearly discernible altered grain parts around pores and along rims.

LUCO 1 is largely featureless with right and interior parts showing an intricate secondary zonation pattern.

(4) Weak zonation with minor alteration features:

DUTH 2 displays only weak remnants of sector-like zonation.

KLEM 3 shows weak remnants of oscillatory zonation that is cut and transitions in places into a diffuse pattern.

SALZ 2 shows remains of sector-like combined with complex zonation.

(5) Weak zonation with strong alteration features:

DURO 2 displays remnants of oscillatory zonation.

DUTH 3 has partly preserved oscillatory zonation with parts of the grain having a diffuse pattern.

GRAESER 1 shows remains of sector combined with oscillatory zonation, but strong zonation in the altered parts of the crystal.

GRAESER 4 shows remnants of sector zonation and has very low Th contents of just below 1100 ppm and elevated common Pb contents below 20%.

KLEM 2 has a diffuse internal structure and elevated common Pb contents that remain below 21%.

TAMB 1 has Th (>3300 ppm) contents that do not allow the identification of clear chemical groups. Weighted mean ages could therefore only be calculated for spots located in close proximity that give a similar age. While most of the measurements have common Pb contents of >5%, five measurements show very high contents of 72-96%, but despite this appear undisturbed.

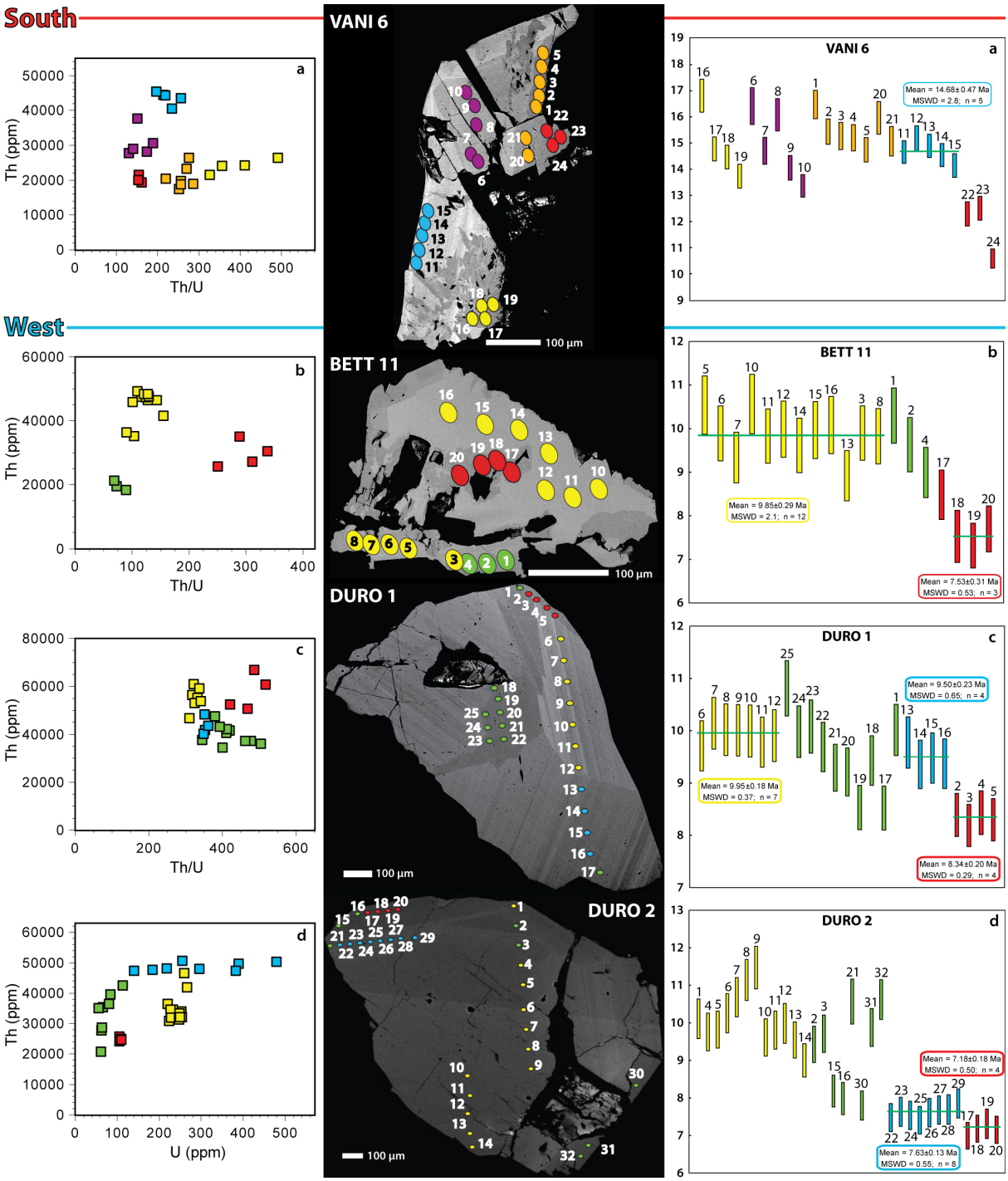

Figure 5. Visualization by sample of all SIMS analyses conducted for this study. Chemical plots that best show the different groups within a sample (left), BSE images(center) with colored ovals representing analysis spots being to scale, age diagrams (right) show $^{208}Pb/^{232}Th$ ages.

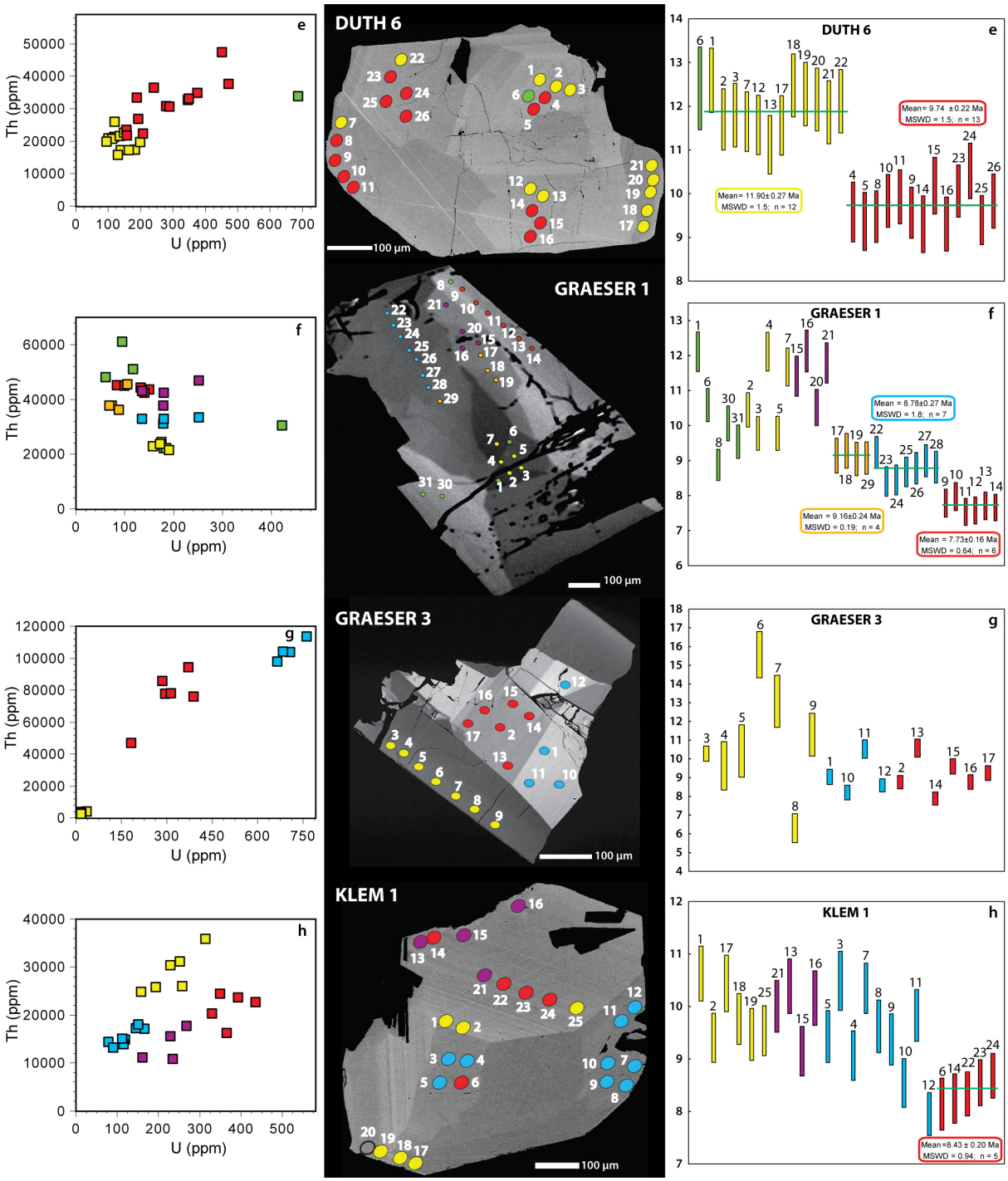

Figure 5. Visualization by sample of all SIMS analyses conducted for this study. Chemical plots that best show the different groups within a sample (left), BSE images(center) with colored ovals representing analysis spots being to scale, age diagrams (right) show $^{208}Pb/^{232}Th$ ages.

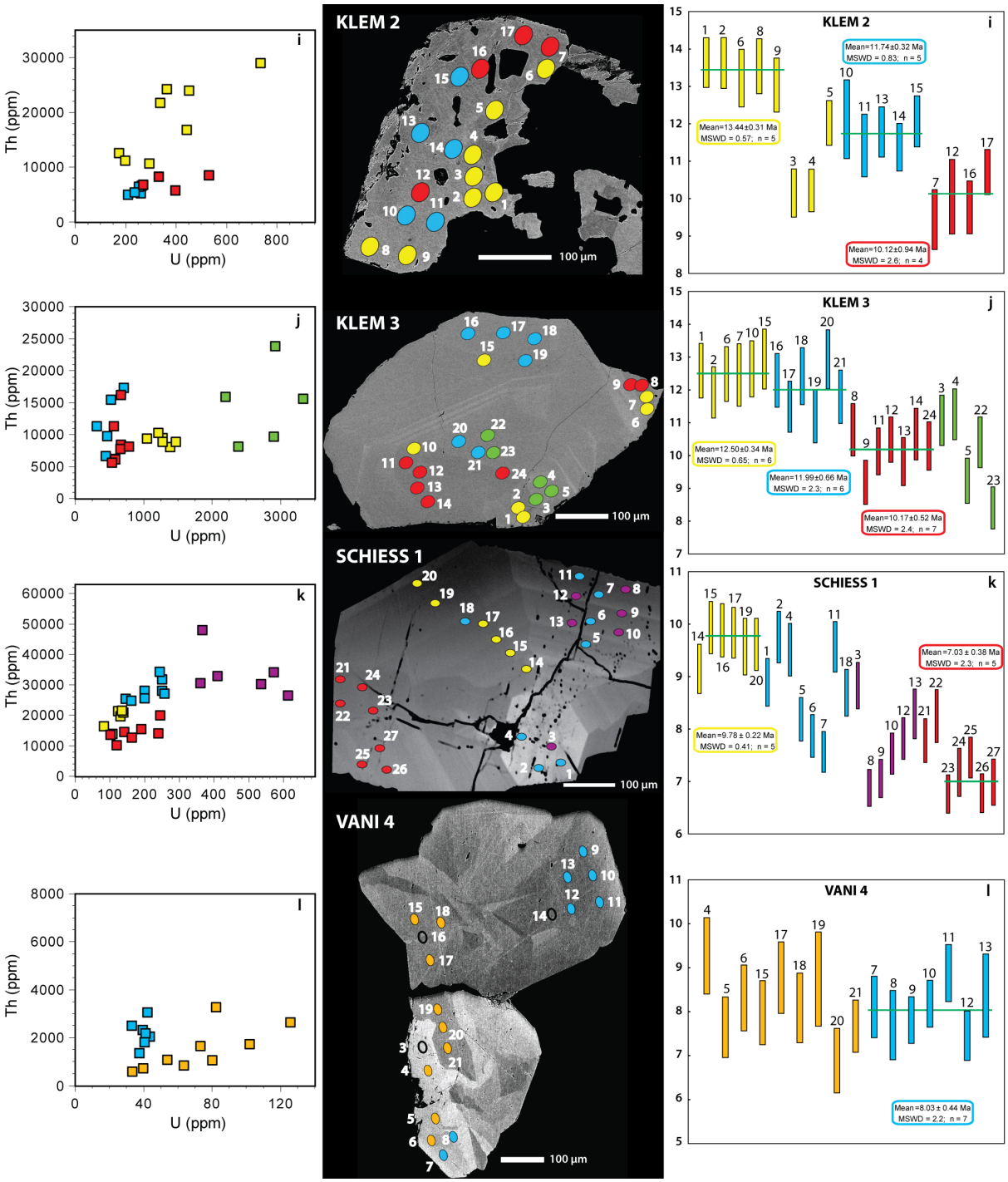

Figure 5. Visualization by sample of all SIMS analyses conducted for this study. Chemical plots that best show the different groups within a sample (left), BSE images(center) with colored ovals representing analysis spots being to scale, age diagrams (right) show $^{208}Pb/^{232}Th$ ages.

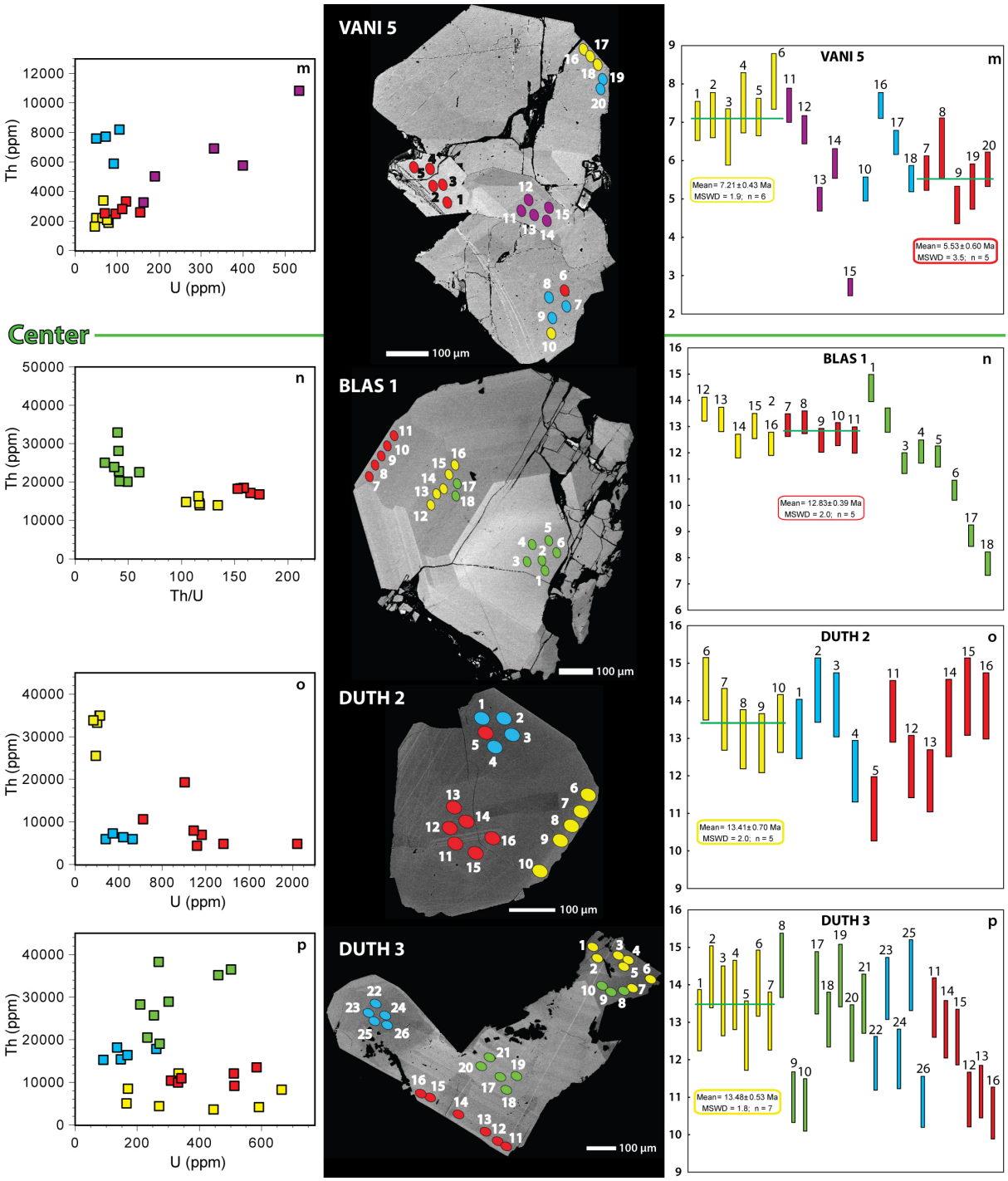

Figure 5. Visualization by sample of all SIMS analyses conducted for this study. Chemical plots that best show the different groups within a sample (left), BSE images(center) with colored ovals representing analysis spots being to scale, age diagrams (right) show $^{208}Pb/^{232}Th$ ages.

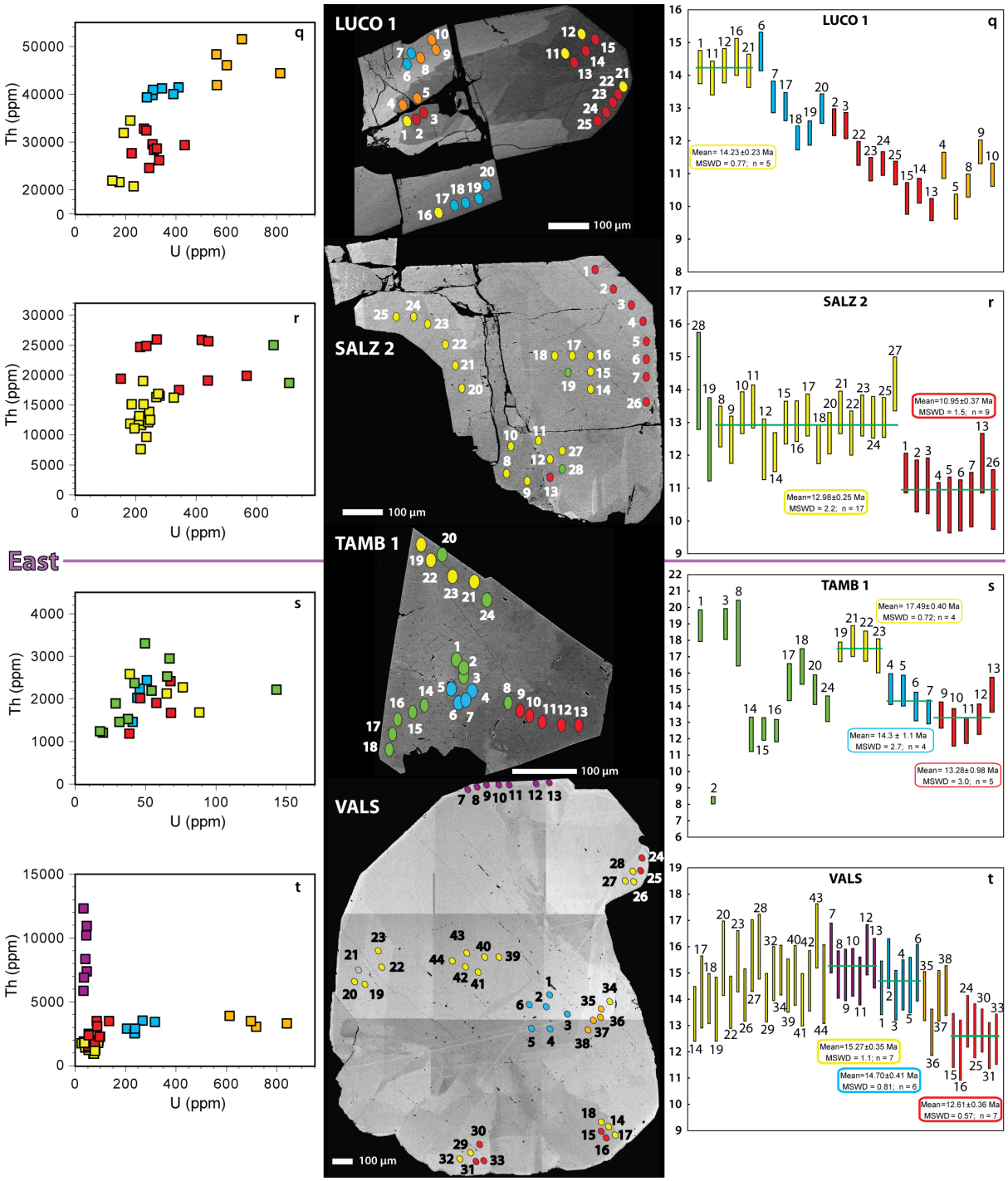

Figure 5. Visualization by sample of all SIMS analyses conducted for this study. Chemical plots that best show the different groups within a sample (left), BSE images(center) with colored ovals representing analysis spots being to scale, age diagrams (right) show $^{208}Pb/^{232}Th$ ages.

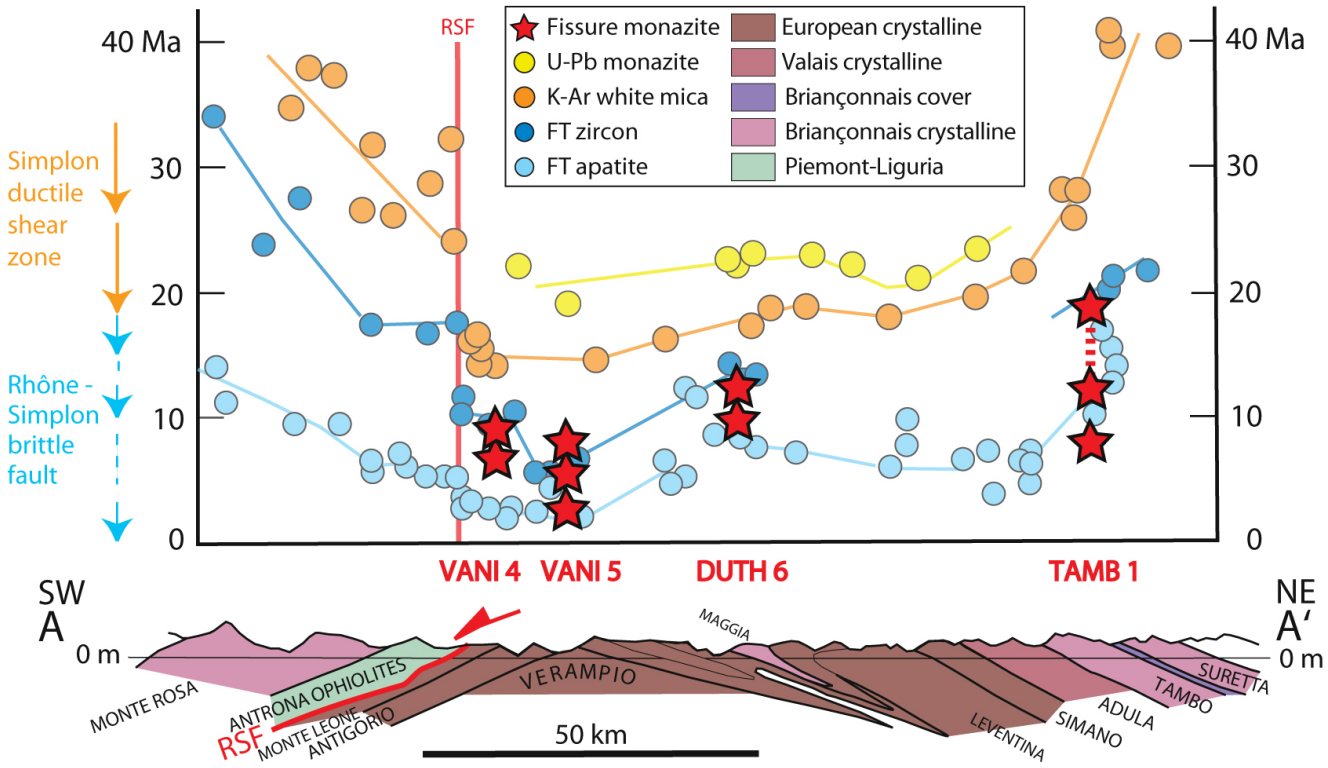

Figure 6. Figure modified from Steck *et al.* (2013), with cooling ages compiled by Steck and Hunziker (1994), and completed with data from Keller *et al.* (2005), Rahn (2005), Elfert *et al.* (2013) and Boston *et al.* (2017). Cleft monazite crystallization ages of samples from this study, located in the vicinity of the cross section (Figs. 1, 2 are shown for comparison. Note that monazite from rocks gives T-max, considerably higher than the crystallization temperature of the hydrothermal cleft/fissure monazite-(Ce) variety.

5 Hydrothermal monazite-(Ce) ages compared to thermochronometry

Hydrothermal monazite-(Ce) crystallization and alteration occur typically in a temperature window of ca. 350 – 200 °C (Gnos *et al.*, 2015; Bergemann *et al.*, 2017, 2018) independent of the local cooling rate. In many areas the oldest recorded hydrothermal monazite-(Ce) ages are predated by $^{40}Ar/^{39}Ar$ white mica cooling ages, and are slightly predated by to coincide with ZFT ages (Gnos *et al.*, 2015; Grand′Homme *et al.*, 2016; Bergemann *et al.*, 2017, 2019; Ricchi *et al.*, 2019). This sequence is also found in most parts of the Lepontine Dome as shown for samples located in vicinity of the NE-SW cross section (Fig. 6), based on Steck *et al.*, (2013). Moreover, it is also well visible in (Fig. 6) that monazite in clefts starts to crystallize much later than monazite in the metamorphic rocks (data from Köppel and Grünenfelder, 1975, and Boston *et al.*, 2017).

A comparison of monazite-(Ce) crystallization ages with ages obtained with thermochronometers, whose closure temperatures depend on the cooling rate, seems to allow the identification of areas experiencing low cooling rates at the time of hydrothermal monazite growth. In such cases, monazite has a larger time window to record tectonic activity, and $^{40}Ar/^{39}Ar$

white mica ages coincide with the beginning of the monazite-(Ce) age record and ZFT ages coincide with or even postdate the youngest found monazite-(Ce) ages. This is the case in (1) the central region of the study area, where the youngest white mica cooling ages of 15.1 $\pm$ 0.70 to 16.30 $\pm$ 0.23 Ma (Allaz *et al.*,2011) located west of sample DUTH 2 and south of sample LUCO 1 (Fig. 1) coincide with the earliest monazite-(Ce) crystallization dated at ca. 14.3 to 14.7 Ma, and ZFT ages of 9.7 $\pm$ 0.5 Ma Ma (Janots *et al.* 2009) coincide with the late phase of monazite-(Ce) age recording around 10 Ma. Also (2) in the vicinity of sample VANI 6 south of the RSF (Fig. 1) the ZFT ages, ranging from 12.0 $\pm$ 2.6 to 7.1 $\pm$ 1.6 Ma (Keller *et al.*, 2005), overlap with the youngest monazite-(Ce) spot ages of around 12.5 to 10.6 Ma. There are no ^{40}Ar/^{39}Ar white mica ages in direct vicinity of VANI 6. However, the sample is located in an area that does not show the jump in cooling ages found along the rest of the brittle Rhone-Simplon Fault bordering the Lepontine Dome to the west (Keller *et al.*, 2005; Campani *et al.*, 2010). A similar age pattern was also found outside the study area, in (3) the Eastern Alps in Austria, in an area affected by Cretaceous Eo-Alpine Barrow-type metamorphism (Bergemann *et al.*, 2018). There, primary monazite-(Ce) mean ages of 90.6 $\pm$ 1.3 to 89.2 $\pm$ 1.8 Ma coincide with ^{40}Ar/^{39}Ar white mica ages of 88.4 $\pm$ 0.4 to 84.3 $\pm$ 0.7 Ma (Dallmeyer *et al.*, 1996) and the youngest monazite spot ages of around 70 Ma coincide with ZFT ages that show a considerable spread of ca.70-50 Ma (Kurz *et al.*, 2011; van Gelder *et al.*, 2015). The three areas have in common that exhumation/cooling rates were low (Steck *et al.*, 2013; Fügenschuh *et al.*, 2000) during the time of hydrothermal monazite-(Ce) crystallization.

Due to the slow cooling rates, the Ar system closure and the end of fission track annealing would have occurred at the lower end of their respective temperature windows, while monazite-(Ce) crystallization presumably occurred during this ca. 350-200 °C temperature window (Gnos *et al.*, 2015; Bergemann *et al.*, 2017, 2018). This may indicate that the coincidence of ^{40}Ar/^{39}Ar white mica ages with the beginning of monazite-(Ce) crystallization and ZFT ages overlapping with the latest hydrothermal monazite-(Ce) crystallization can be used as an indicator of slow exhumation/cooling rates during ongoing tectonic activity.

6 Monazite-(Ce) ages and late Lepontine Dome evolution

Hydrothermal cleft monazite-(Ce) crystallization and dissolution-reprecipitation varied in space and time in the study region as it passed through the monazite-(Ce) crystallization recording window. The growth duration recorded by the spot age range within individual monazite-(Ce) crystals spans from 2.5 Ma to 7 Myr (Table 2, Fig. 5). The total age range of all grains covers the time from *ca.* 19 to 2.7 Ma.

The monazite-(Ce) age record starts in the eastern region (Fig. 1) of the study area at the edges of the Lepontine Dome (Fig. 7a), with the earliest ages around 19 Ma (sample TAMB 1; Figs. 4, 5s), slightly postdated by sample VALS somewhat to the north of TAMB 1 at $\sim$16.5 Ma (Fig. 5t). While the age record continues in the east, it starts in the Central region (Fig. 1) around 14.7 - 14.3 Ma. The parallel monazite-(Ce) age record for the central and eastern regions continues until *ca.* 12.5 Ma after which it ends in the east, with the exception of isolated spot ages of $\sim$8.3 Ma in the east (TAMB 1) and 7.8 Ma in the center (BLAS 1). The western area (Fig. 1) has a more heterogeneous age record with starting dates being diachronous within the area from east to west/south-west (Figs. 7b-e). The oldest ages are around 13.6 Ma (KLEM 2) with the area in which ages are recorded progressively spreading west, until by ca. 10 Ma most samples from the western region record ages. After this,

the age record ends first in the central region and then the easternmost western region at *ca.* 9.5 Ma. The record continues in most of the western region (Fig. 7e), until it becomes progressively more localized by ∼7.5 towards the west and the vicinity of the Rhone-Simplon Fault system (Fig. 7f). The youngest widely recorded monazite-(Ce) age group for this area dates to around 7 Ma (Fig. 7f), and only one sample (VANI 5) records ages down to around 5 Ma, with a single spot age of ∼2.7 Ma. The southern region (Fig. 1) at the very edge of the Lepontine Dome, separated from most of the Western region by the Rhone-Simplon Fault, shows a similar age range as the eastern region. As in the east, the monazite-(Ce) age record starts early at ca. 16.8 Ma and continues somewhat further down to around 10.6 Ma (Fig. 5a-d).

Overall, the monazite-(Ce) chronologic record shows a clear east-west trend without large age jumps within the Lepontine Dome. The record starts in the eastern- (and southern) parts of the study area, with the activity then moving through the central to the western area, where it progressively concentrates on the large fault systems in the west of the Lepontine Dome.

The oldest recorded monazite-(Ce) ages were found in the eastern area (TAMB 1; Fig. 1) and fall into two groups, around 19 Ma and a mean age at 17.49 ± 0.4 Ma (Figs. 4, Tab. 2), during which time the area around TAMB 1 experienced a time of rapid exhumation and cooling (Steck and Hunziker, 1994). The nearby Forcola Fault (Fig. 1) was estimated to have been active sometime around 25-18 Ma on the basis of Rb-Sr and K-Ar cooling ages (Meyre *et al.*, 1998). In this context, the monazite-(Ce) ages would date the final deformation phases of such normal faults as the Forcola Fault. Notably, these faults, and possibly the Forcoloa Fault itself, may have been active far longer, as suggested by monazite-(Ce) ages down to ∼8.3 Ma (Figs. 5s, Tab. 2). The youngest ages even postdate apatite fission track ages (AFT; Fig. 6), which may have been facilitated by the late circulation of hot fluids, something which could be shown for hydrothermal monazite-(Ce) of the Lauziere and Mont Blanc Massifs (Janots *et al.*, 2019; Bergemann *et al.*, 2019). North of TAMB 1, the sample VALS age record starts slightly later at ∼16.5 Ma that then runs parallel to that of TAMB 1 (Figs. 5s, t).

In the central area close to the sample locations, temperatures were still prograde up until the time of 19-18 Ma at 450-430°C (Janots *et al.*, 2009) as deduced from allanite dating. After this time, conditions must have decreased to lower temperatures during exhumation, as the hydrothermal monazite-(Ce) age record started after around 16-15 Ma in the Gotthard Nappe and eastern Lepontine Dome (Fig. 7b) and continued to later than ∼13 Ma (Fig. 7c). After this time the age record receded from the eastern region, which cooled below 180°C around 12 Ma (e.g. Price *et al.*, 2018, zircon U/Th-He), and the Gotthard Nappe west- and southwards into the Lepontine Dome. This would date the decoupling of the Gotthard Nappe which experienced a rapid exhumation due to steepening during backfolding (Wiederkehr *et al.*, 2009; Ricchi *et al.*, 2019) from the Lepontine Dome to *ca.* 13-12 Ma, as the samples of the central area south of the Gotthard Nappe show a continued widespread age record down to ∼9 Ma (Fig. 7d). During this time interval (Fig. 7c) primary monazite-(Ce) crystallizes also along the rest of the extended Rhone-Simplon Fault system (Grand′Homme *et al.*, 2016; Bergemann *et al.*, 2017, 2019; Ricchi *et al.*, 2019). Where it dates in some areas a switch from thrusting/transtensional movements to pure strike-slip deformation through the formation of a new cleft generation with a different orientation associated with strong hydrothermal fluid activity (Bergemann *et al.*, 2017, 2019; Janots *et al.*,2019). Since in the study area clefts outside the Gotthard Nappe, where they are horizontal, are vertical whether they formed during extension or later strike-slip deformation, such a switch in deformation style cannot be proven. But it might

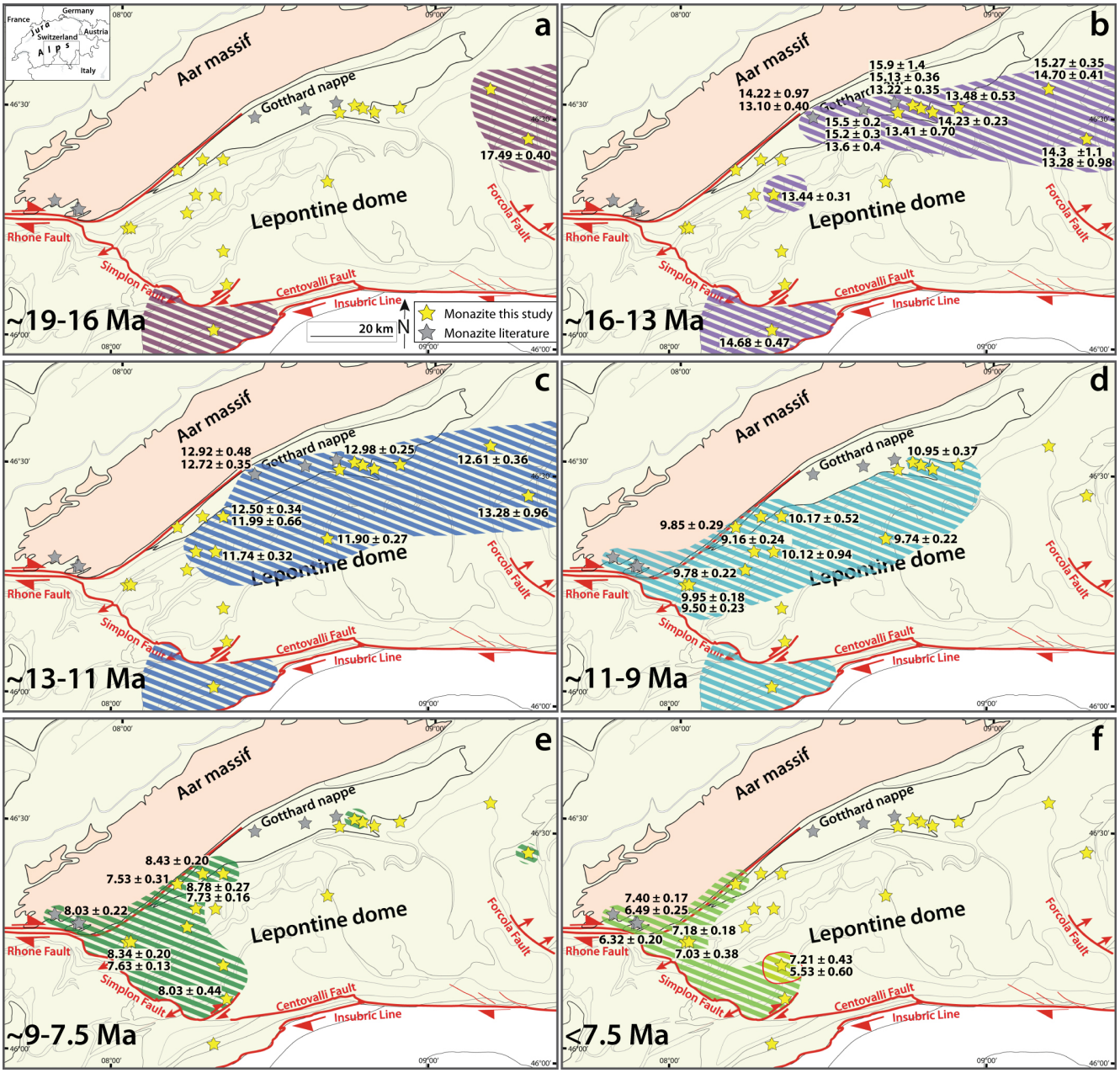

Figure 7. Overview maps of the study area showing the monazite-(Ce) age record over time and space. Note the shift over time from the southern and eastern regions of the Lepontine Dome to the central and western areas and finally to the areas close to the shear zones bounding its western limit. Weighted mean ages, quoted near the stars representing the corresponding sample locations, indicate individual deformation events that could be identified for a grain within a given time interval. Published hydrothermal monazite-(Ce) locations (grey stars) of the areas adjacent to the Lepontine Dome are from Janots *et al.* (2012), Berger *et al.* (2013) and Ricchi *et al.* (2019).

explain the progressive restriction of the monazite-(Ce) age record areas to samples from the vicinity of major fault zones in the western Lepontine Dome (Figs. 7d-f).

11 Ma (Fig. 7d) marks the end of the hydrothermal monazite-(Ce) age record in the hanging wall of the Rhone-Simplon Fault (southern region, Fig. 1) which had continued since ∼16.8 Ma, largely parallel to that in the eastern region (Figs. 7a-d). At the same time, 11-10 Ma also marks the beginning of monazite-(Ce) crystallization in the foot wall of the Rhone-Simplon Fault ((Figs. 1, 7d). The primary monazite-(Ce) crystallization ages of the western area tend to postdate, but are still in close agreement with zircon fission track ages (Fig. 6). Samples of the western region often yield well constrained weighted mean ages (Fig. 5), which might suggest a dominance of strong individual tectonic events. This in mind, weighted mean ages in the western zone (Fig. 4) may suggest deformation during brittle tectonics along the extended Rhone-Simplon Fault system.

The mean age group around 12 Ma, found in the eastern part of the western zone (Figs. 4, 7c) is related to the exhumed deeper part of the Simplon Fault (Hartel and Herwegh 2012), whereas the younger ages are more close to the localized and late Simplon Fault. The 12 Ma age also falls together with the switch in deformational style elsewhere in the Western Alps discussed above, and is followed by a group from ∼10-7 Ma (Figs. 4, 7d). These two age groups are also recorded in the central Lepontine (sample DUTH 6; Fig. 5e). After 10 Ma, the weighted mean ages show a spread down to *ca.* 7 Ma but are progressively restricted to the westernmost areas close to the fault zones (Figs. 4, 7e, f). The ages likely mark phases of tectonic activity and corroborate evidence of continuing deformation along the Rhone-Simplon Fault (e.g. Zwingmann and Mancktelow, 2004; Campani *et al.*, 2010; Surace *et al.*, 2011). Only one sample in this group (VANI 5; Fig. 7f) yields ages younger than *ca.* 7 Ma, with a weighted mean age around 5.5 Ma and a spot age of ∼2.7 Ma (Fig. 5m). The sample comes from an area where strong late-stage hydrothermal activity occurred, and the ∼ 5.5 Ma age coincides with ZFT ages of 6.4-5.4 Ma that are younger than those found in most of the region (Keller *et al.*, 2006). This coincidence of ages younger than in the surrounding areas may indicate a resetting of the ZFT ages through the hydrothermal activity. These phases of strike-slip deformation are not local to the western Lepontine Dome, but seem to have affected the extended Rhone-Simplon Fault system in much of the Western Alps (Berger *et al.*, 2013; Grand′Homme *et al.*, 2016; Bergemann *et al.*, 2017, 2019; Ricchi *et al.*, 2019).

7 Summary

Hydrothermal fissure monazite-(Ce) offers the possibility to date tectonic activity in the brittle domain for extended time periods, as it could be shown to provide a record of the shifting tectonic activity within the Lepontine Dome associated with the regionsal exhumation history. A comparison between hydrothermal monazite-(Ce) samples from different parts of the Lepontine Dome and thermo-chronometric data suggest that hydrothermal monazite-(Ce) dating might be used to identify areas of slow exhumation/cooling rates during ongoing tectonic activity. The ^{232}Th-^{208}Pb monazite-(Ce) crystallization data records prolonged hydrothermal activity between ∼19 and 2.7 Ma, and contribute to the understanding of the tectonic evolution of the Central Alps in a temperature range of roughly 350-200°C. The monazite-(Ce) age record reveals a relatively smooth east-west age trend within the Lepontine Dome. The record starts in the eastern- (and southern) parts of the study area, with

the recorded activity then moving through the central to the western area, where it progressively concentrates on the large fault systems of the western Lepontine Dome. The oldest ages of ∼19-17 Ma come from the eastern- and southernmost regions of the study area, in the hanging wall of the Forcola and Rhone-Simplon normal faults. Within the dome, monazite-(Ce) crystallization started in the eastern Lepontine Dome, as well as the eastern Gotthard Nappe around 16-15 Ma. Further west, primary crystallization occurred in the western Gotthard nappe at 13-10 Ma. Younger ages of 9-7 Ma in the west of the study area record the progressive restriction of the recorded tectonic activity to the extended Rhone-Simplon Fault system.

Appendix A: Appendix A

Sample	Analysis ID	U ppm	Th ppm	Pb ppm	Th/U meas	$^{204}Pb/^{208}Pb$	$\pm\sigma$ %	$^{232}Th^{143}Nd^{16}O_2^{++}/^{208}Pb$	$\pm\sigma$ %	f208	$\pm\sigma$ %	$^{208}Pb/^{232}Th$ uncorr.	$\pm\sigma$ %	$^{208}Pb/^{232}Th$ Age corr. (Ma)	$\pm\sigma$ Ma
BETT11															
Group A	n5245mnzBett11-03	339	35153	104	3,6	0,00196	5,6	0,000285	16	0,05	0,00	0,00052	3,3	9,91	0,31
	n5245mnzBett11-05	323	46322	143	4,4	0,00179	4,6	0,000375	12	0,04	0,00	0,00054	3,3	10,55	0,33
	n5245mnzBett11-06	406	47398	117	5,0	0,00157	6,0	0,000325	18	0,04	0,00	0,00051	3,3	9,91	0,31
	n5245mnzBett11-07	454	45846	101	4,3	0,00234	6,4	0,000224	20	0,07	0,01	0,00050	3,3	9,36	0,29
	n5245mnzBett11-08	401	36308	91	4,0	0,00173	6,2	0,000261	18	0,05	0,00	0,00051	3,4	9,84	0,32
	n5245mnzBett11-10	267	41536	155	3,9	0,00158	4,9	0,000467	10	0,03	0,00	0,00054	3,3	10,58	0,34
	n5245mnzBett11-11	363	46418	128	5,4	0,00154	5,7	0,000294	13	0,04	0,00	0,00051	3,3	9,84	0,31
	n5245mnzBett11-12	379	47217	125	5,7	0,00110	6,6	0,000288	14	0,02	0,00	0,00051	3,3	10,00	0,32
	n5245mnzBett11-13	448	49209	110	5,3	0,00104	9,0	0,000135	28	0,03	0,00	0,00046	3,3	8,94	0,29
	n5245mnzBett11-14	368	47595	129	4,6	0,00119	8,1	0,000163	22	0,03	0,00	0,00049	3,3	9,63	0,31
	n5245mnzBett11-15	399	48319	121	5,6	0,00115	8,0	0,000361	16	0,02	0,00	0,00050	3,3	9,98	0,33
	n5245mnzBett11-16	377	48294	128	5,6	0,00138	6,7	0,000270	17	0,03	0,00	0,00052	3,3	10,09	0,33
Group B	n5245mnzBett11-17	87	27100	311	1,2	0,00122	12,3	0,000225	31	0,03	0,01	0,00043	3,4	8,50	0,28
	n5245mnzBett11-18	103	25696	251	0,7	0,00323	10,4	0,000321	30	0,10	0,01	0,00042	4,1	7,55	0,30
	n5245mnzBett11-19	90	30321	338	0,9	0,00198	12,3	0,000176	45	0,06	0,01	0,00039	3,6	7,34	0,26
	n5245mnzBett11-20	121	34890	289	1,8	0,00112	13,1	0,000288	28	0,02	0,01	0,00039	3,4	7,72	0,26
Group C	n5245mnzBett11-01	203	18179	90	1,4	0,00411	4,7	0,000403	17	0,13	0,01	0,00059	3,4	10,31	0,31
	n5245mnzBett11-02	266	19386	73	2,2	0,00193	8,0	0,000235	25	0,06	0,01	0,00051	3,3	9,65	0,31
	n5245mnzBett11-04	306	21220	69	2,4	0,00229	7,8	0,000286	24	0,07	0,01	0,00048	3,4	9,01	0,29
BLAS1															
Group A	n5242mnzBlas1-07	96	16621	173	1,5	0,00214	6,7	0,000270	24	0,06	0,01	0,00069	1,6	13,08	0,22
	n5242mnzBlas1-08	103	17013	165	1,6	0,00210	7,2	0,000275	22	0,06	0,01	0,00069	1,6	13,19	0,22
	n5242mnzBlas1-09	117	18246	155	1,8	0,00214	8,0	0,000302	24	0,06	0,01	0,00066	1,8	12,50	0,23
	n5242mnzBlas1-10	116	18413	159	1,8	0,00203	7,7	0,000284	32	0,06	0,01	0,00067	1,7	12,74	0,22
	n5242mnzBlas1-11	119	18159	153	1,9	0,00212	12,3	0,000136	42	0,07	0,01	0,00067	1,8	12,52	0,25
Group B	n5242mnzBlas1-12	103	13819	134	1,6	0,00193	7,4	0,000243	24	0,06	0,01	0,00072	1,6	13,69	0,23
	n5242mnzBlas1-13	118	13886	117	1,7	0,00172	8,4	0,000173	30	0,05	0,01	0,00070	1,7	13,30	0,23
	n5242mnzBlas1-14	140	14653	105	2,1	0,00192	9,0	0,000261	27	0,05	0,01	0,00064	1,8	12,29	0,22
	n5242mnzBlas1-15	122	14275	117	1,7	0,00172	13,0	0,000128	32	0,06	0,01	0,00068	1,7	13,04	0,24
	n5242mnzBlas1-16	140	16210	116	1,9	0,00206	9,4	0,000104	46	0,07	0,01	0,00066	1,7	12,37	0,22
Unaligned	n5242mnzBlas1-01	408	20051	49	4,3	0,00124	9,0	0,000308	12	0,02	0,00	0,00074	1,8	14,49	0,26
	n5242mnzBlas1-02	552	22751	41	5,4	0,00091	9,3	0,000246	17	0,02	0,00	0,00067	1,7	13,27	0,23
	n5242mnzBlas1-03	818	32828	40	8,2	0,00069	10,0	0,000165	22	0,01	0,00	0,00058	1,7	11,64	0,20
	n5242mnzBlas1-04	684	27995	41	6,9	0,00067	10,5	0,000200	21	0,01	0,00	0,00060	1,8	12,08	0,22
	n5242mnzBlas1-05	648	23824	37	5,7	0,00154	9,6	0,000246	22	0,04	0,01	0,00061	1,6	11,89	0,20
	n5242mnzBlas1-06	894	24891	28	6,5	0,00091	11,9	0,000120	32	0,03	0,00	0,00054	1,8	10,60	0,19
	n5242mnzBlas1-17	370	22459	61	4,1	0,00097	17,7	0,000109	58	0,03	0,01	0,00045	2,3	8,88	0,20
	n5242mnzBlas1-18	480	20135	42	4,5	0,00088	25,7	b.d.	b.d.	0,03	0,01	0,00040	2,8	7,82	0,22
DURO1															
Group A	n4202-Duro1@06	311	46600	150	23	0,00190	6,5	0,000331	18	0,05	0,01	0,00051	2,5	9,73	0,24
	n4202-Duro1@07	318	56364	177	29	0,00151	6,1	0,000208	21	0,04	0,00	0,00052	2,5	10,15	0,25
	n4202-Duro1@08	322	60912	189	31	0,00172	5,3	0,000361	13	0,04	0,00	0,00052	2,5	10,03	0,25
	n4202-Duro1@09	338	59120	175	30	0,00150	6,6	0,000250	15	0,04	0,00	0,00052	2,5	10,02	0,25
	n4202-Duro1@10	333	55057	165	28	0,00162	7,3	0,000329	15	0,04	0,00	0,00051	2,5	10,01	0,25
	n4202-Duro1@11	326	53025	163	26	0,00177	5,9	0,000293	14	0,05	0,00	0,00051	2,5	9,79	0,24
	n4202-Duro1@12	341	53812	158	27	0,00154	6,2	0,000379	14	0,03	0,00	0,00051	2,5	9,92	0,25
Group B	n4202-Duro1@02	469	50660	108	32	0,00123	9,0	0,000128	35	0,04	0,00	0,00043	2,5	8,41	0,21
	n4202-Duro1@03	518	60715	117	44	0,00134	8,9	0,000202	31	0,04	0,01	0,00042	2,5	8,21	0,20
	n4202-Duro1@04	487	66762	137	46	0,00122	9,1	0,000262	21	0,03	0,00	0,00043	2,5	8,45	0,21
	n4202-Duro1@05	422	52298	124	34	0,00147	8,3	0,000136	35	0,05	0,01	0,00043	2,5	8,31	0,20
	n4202-Duro1@13	352	48197	137	24	0,00136	6,9	0,000383	16	0,02	0,00	0,00050	2,5	9,79	0,24
	n4202-Duro1@14	353	41755	118	20	0,00151	7,5	0,000217	19	0,04	0,00	0,00048	2,5	9,37	0,23
	n4202-Duro1@15	349	40100	115	19	0,00147	9,0	0,000401	16	0,03	0,01	0,00048	2,5	9,49	0,24
	n4202-Duro1@16	362	43377	120	20	0,00156	10,0	0,000353	17	0,03	0,01	0,00048	2,5	9,38	0,24

Sample	Analysis ID	U ppm	Th ppm	Pb ppm	Th/U meas	$^{204}Pb/^{208}Pb$	$\pm\sigma$ %	$^{232}Th^{143}Nd^{16}O_2^{++}/^{208}Pb$	$\pm\sigma$ %	f208	$\pm\sigma$ %	$^{208}Pb/^{232}Th$ uncorr.	$\pm\sigma$ %	$^{208}Pb/^{232}Th$ Age corr. (Ma)	$\pm\sigma$ Ma
Unaligned	n4202-Duro1@01	345	37553	109	19	0,00233	7,1	0,000257	19	0,07	0,01	0,00053	2,5	10,03	0,24
	n4202-Duro1@17	380	47381	125	24	0,00134	8,3	0,000208	23	0,04	0,00	0,00044	2,5	8,54	0,21
	n4202-Duro1@18	419	41426	99	20	0,00166	7,6	0,000330	19	0,04	0,01	0,00049	2,5	9,45	0,24
	n4202-Duro1@19	504	36012	71	27	0,00199	10,7	0,000111	41	0,07	0,01	0,00045	2,5	8,55	0,21
	n4202-Duro1@20	401	34299	86	21	0,00200	8,5	0,000336	22	0,05	0,01	0,00048	2,5	9,23	0,23
	n4202-Duro1@21	411	40448	98	27	0,00207	6,8	0,000174	26	0,07	0,01	0,00049	2,5	9,31	0,22
	n4202-Duro1@22	412	42030	102	28	0,00186	6,9	0,000225	22	0,05	0,01	0,00051	2,5	9,70	0,24
	n4202-Duro1@23	393	43050	110	29	0,00183	6,6	0,000271	20	0,05	0,01	0,00056	2,5	10,82	0,26
	n4202-Duro1@24	478	37122	78	30	0,00187	8,9	0,000123	45	0,06	0,01	0,00053	2,5	9,99	0,25
	n4202-Duro1@25	463	37225	80	29	0,00210	8,5	0,000207	29	0,07	0,01	0,00053	2,6	10,09	0,25
DURO2															
Group A	n4203-Duro2@1	249	33286	133	16	0,00123	9,2	0,000608	15	0,00	0,01	0,00050	2,6	10,13	0,26
	n4203-Duro2@04	221	36462	165	16	0,00196	7,3	0,000450	20	0,04	0,01	0,00050	2,6	9,78	0,25
	n4203-Duro2@05	254	33837	133	15	0,00194	7,2	0,000299	19	0,05	0,01	0,00051	2,6	9,84	0,25
	n4203-Duro2@06	233	34523	148	16	0,00190	7,7	0,000372	18	0,05	0,01	0,00053	2,6	10,27	0,26
	n4203-Duro2@07	228	34559	152	15	0,00211	6,7	0,000314	22	0,06	0,01	0,00056	2,5	10,71	0,26
	n4203-Duro2@08	224	30753	137	14	0,00157	7,6	0,000320	19	0,04	0,01	0,00057	2,5	11,16	0,27
	n4203-Duro2@09	229	31883	139	15	0,00170	7,1	0,000438	16	0,03	0,01	0,00059	2,5	11,48	0,28
	n4203-Duro2@10	248	31190	126	14	0,00180	9,2	0,000303	22	0,05	0,01	0,00050	2,6	9,63	0,25
	n4203-Duro2@11	255	31988	126	14	0,00164	10,9	0,000304	20	0,04	0,01	0,00051	2,6	9,83	0,25
	n4203-Duro2@12	250	32112	128	16	0,00308	8,8	0,000393	18	0,09	0,01	0,00054	2,7	10,00	0,27
	n4203-Duro2@13	267	41854	157	19	0,00134	9,1	0,000386	17	0,02	0,01	0,00048	2,5	9,56	0,24
	n4203-Duro2@14	261	46526	179	22	0,00140	8,1	0,000179	25	0,04	0,00	0,00047	2,5	9,03	0,22
Group B	n4203-Duro2@17	106	25722	243	17	0,00101	18,8	0,000000	71	0,04	0,01	0,00036	2,5	7,02	0,18
	n4203-Duro2@18	106	24182	227	17	0,00061	25,9	0,000000	50	0,02	0,01	0,00037	2,5	7,21	0,18
	n4203-Duro2@19	110	24889	226	19	0,00082	29,3	0,000280	38	0,01	0,01	0,00037	2,5	7,34	0,20
	n4203-Duro2@20	110	24569	223	19	0,00045	22,1	0,000157	58	0,01	0,01	0,00036	2,5	7,18	0,18
Group C	n4203-Duro2@22	141	47357	336	32	0,00122	12,3	0,000185	33	0,03	0,01	0,00038	2,5	7,50	0,19
	n4203-Duro2@23	184	47581	258	39	0,00075	14,8	0,000244	30	0,01	0,01	0,00038	2,5	7,66	0,19
	n4203-Duro2@24	218	47995	220	42	0,00079	18,7	0,000000	50	0,03	0,01	0,00039	2,5	7,56	0,19
	n4203-Duro2@25	256	50591	198	41	0,00100	13,7	0,000000	45	0,04	0,01	0,00038	2,5	7,43	0,18
	n4203-Duro2@26	296	47845	161	43	0,00087	17,4	0,000068	58	0,03	0,01	0,00039	2,5	7,64	0,19
	n4203-Duro2@27	390	49666	127	45	0,00078	15,5	0,000000	41	0,03	0,00	0,00039	2,5	7,70	0,19
	n4203-Duro2@28	480	50223	105	45	0,00065	17,4	0,000211	33	0,01	0,01	0,00039	2,5	7,72	0,20
	n4203-Duro2@29	382	47275	124	30	0,00098	12,4	0,000062	51	0,03	0,00	0,00040	2,5	7,88	0,19
Unaligned	n4203-Duro2@02	56	35069	624	15	0,00133	9,8	0,000273	26	0,03	0,01	0,00048	2,6	9,45	0,24
	n4203-Duro2@03	64	28686	449	13	0,00114	9,8	0,000423	17	0,01	0,01	0,00049	2,5	9,73	0,25
	n4203-Duro2@15	63	27636	439	13	0,00122	12,5	0,000291	28	0,03	0,01	0,00042	2,6	8,21	0,21
	n4203-Duro2@16	62	20762	334	10	0,00159	15,2	0,000254	33	0,04	0,01	0,00041	2,6	8,01	0,21
	n4203-Duro2@21	66	35309	535	no data	0,00275	10,1	0,000390	21	0,08	0,01	0,00057	2,8	10,59	0,30
	n4203-Duro2@30	113	42468	374	22	0,00106	14,4	0,000089	40	0,03	0,01	0,00040	2,5	7,83	0,19
	n4203-Duro2@31	84	39434	469	17	0,00145	8,0	0,000466	15	0,02	0,01	0,00050	2,5	9,90	0,25
	n4203-Duro2@32	81	36357	450	18	0,00126	7,9	0,000391	16	0,02	0,00	0,00054	2,5	10,64	0,26
DUTH2															
Group A	n5253mnzDuth2-01	282	5858	21	1	0,00365	6,5	0,000281	27	0,12	0,01	0,00075	3,2	13,27	0,39
	n5253mnzDuth2-02	347	7174	21	2	0,00228	8,5	0,000131	38	0,08	0,01	0,00077	3,1	14,30	0,43
	n5253mnzDuth2-03	441	6368	14	2	0,00230	9,2	0,000110	56	0,08	0,01	0,00075	3,2	13,91	0,43
	n5253mnzDuth2-04	529	5925	11	2	0,00258	13,5	0,000236	41	0,08	0,01	0,00065	3,3	12,14	0,41
Group B	n5253mnzDuth2-06	191	25471	134	4	0,00146	4,8	0,000273	12	0,04	0,00	0,00074	3,0	14,34	0,41
	n5253mnzDuth2-07	206	33243	162	5	0,00116	8,2	0,000245	14	0,03	0,00	0,00069	3,1	13,52	0,41
	n5253mnzDuth2-08	227	34916	154	5	0,00122	5,8	0,000263	18	0,03	0,00	0,00066	3,1	12,99	0,39
	n5253mnzDuth2-09	229	34936	152	5	0,00128	5,6	0,000230	15	0,03	0,00	0,00066	3,1	12,89	0,39
	n5253mnzDuth2-10	171	33751	198	4	0,00141	4,6	0,000234	12	0,04	0,00	0,00069	3,0	13,41	0,38
Group C	n5253mnzDuth2-05	1167	6847	6	4	0,00320	14,4	b.d.	b.d.	0,12	0,02	0,00063	3,9	11,15	0,43
	n5253mnzDuth2-11	626	10601	17	3	0,00214	6,1	0,000367	18	0,06	0,01	0,00072	3,1	13,74	0,41

Sample	Analysis ID	U ppm	Th ppm	Pb ppm	Th/U meas	$^{204}Pb/^{208}Pb$	±σ %	$^{232}Th^{143}Nd^{16}O_2^{++}/^{208}Pb$	±σ %	f208	±σ %	$^{208}Pb/^{232}Th$ uncorr.	±σ %	$^{208}Pb/^{232}Th$ Age corr. (Ma)	±σ Ma
	n5253mnzDuth2-12	1121	4363	4	2	0,00251	12,9	0,000173	42	0,08	0,01	0,00066	3,4	12,27	0,41
	n5253mnzDuth2-13	1364	4791	4	2	0,00292	11,1	0,000114	67	0,10	0,01	0,00066	3,6	11,89	0,41
	n5253mnzDuth2-14	2042	4798	2	3	0,00216	19,4	b.d.	b.d.	0,08	0,02	0,00073	3,7	13,56	0,51
	n5253mnzDuth2-15	1090	7896	7	3	0,00167	11,5	0,000237	33	0,05	0,01	0,00073	3,7	14,13	0,51
	n5253mnzDuth2-16	1010	19180	19	6	0,00116	11,2	0,000037	67	0,04	0,01	0,00072	3,3	13,88	0,44
DUTH3															
Group A	n5252mnzDuth3-01	271	4320	16	1	0,00275	9,8	0,000186	40	0,09	0,01	0,00071	3,2	13,07	0,41
	n5252mnzDuth3-02	334	11951	36	3	0,00173	7,5	0,000200	21	0,05	0,01	0,00074	3,0	14,23	0,41
	n5252mnzDuth3-03	447	3576	8	1	0,00484	11,3	0,000201	35	0,17	0,02	0,00081	3,2	13,59	0,46
	n5252mnzDuth3-04	592	4080	7	1	0,00192	16,9	0,000168	50	0,06	0,01	0,00072	3,3	13,74	0,46
	n5252mnzDuth3-05	666	8245	12	3	0,00357	8,0	0,000186	39	0,12	0,01	0,00072	3,9	12,66	0,46
	n5252mnzDuth3-06	167	5038	30	1	0,00275	10,0	0,000365	25	0,08	0,01	0,00076	3,2	14,06	0,44
	n5252mnzDuth3-07	170	8484	50	2	0,00207	7,6	0,000288	24	0,06	0,01	0,00069	3,1	13,05	0,39
Group B	n5252mnzDuth3-11	308	10329	33	2	0,00211	8,9	0,000356	18	0,05	0,01	0,00070	3,0	13,41	0,40
	n5252mnzDuth3-12	511	12054	24	2	0,00144	12,3	0,000167	32	0,04	0,01	0,00057	3,4	10,96	0,36
	n5252mnzDuth3-13	514	9123	18	2	0,00290	7,9	0,000176	33	0,10	0,01	0,00061	3,3	11,17	0,35
	n5252mnzDuth3-14	332	9879	30	2	0,00190	7,1	0,000331	28	0,05	0,01	0,00067	3,0	12,83	0,38
	n5252mnzDuth3-15	342	10842	32	2	0,00223	6,6	0,000312	19	0,06	0,01	0,00067	3,1	12,63	0,37
	n5252mnzDuth3-16	584	13471	23	3	0,00116	12,1	0,000116	41	0,04	0,01	0,00054	3,3	10,61	0,34
Group C	n5252mnzDuth3-22	91	15181	166	1	0,00267	4,9	0,000241	22	0,09	0,01	0,00071	3,0	13,09	0,37
	n5252mnzDuth3-23	135	18092	134	2	0,00169	8,1	0,000174	26	0,05	0,01	0,00062	3,1	11,93	0,36
	n5252mnzDuth3-24	148	15295	103	2	0,00148	11,8	0,000068	45	0,05	0,01	0,00073	3,1	13,92	0,41
	n5252mnzDuth3-25	168	16320	97	2	0,00254	8,3	0,000148	33	0,09	0,01	0,00065	3,5	12,04	0,40
	n5252mnzDuth3-26	262	17756	68	4	0,00125	12,4	0,000167	40	0,04	0,01	0,00073	3,3	14,27	0,47
Unaligned	n5252mnzDuth3-08	233	20389	87	3	0,00162	8,4	0,000135	29	0,05	0,01	0,00057	3,2	10,90	0,34
	n5252mnzDuth3-09	211	28168	134	4	0,00129	8,3	0,000182	24	0,04	0,00	0,00057	3,1	11,03	0,34
	n5252mnzDuth3-10	269	38167	142	6	0,00079	9,7	0,000079	30	0,02	0,00	0,00055	3,3	10,82	0,35
	n5252mnzDuth3-17	255	25683	101	5	0,00140	5,5	0,000321	11	0,03	0,00	0,00072	3,0	14,07	0,41
	n5252mnzDuth3-18	272	19025	70	4	0,00131	8,7	0,000281	18	0,03	0,00	0,00074	3,0	14,53	0,43
	n5252mnzDuth3-19	502	36463	73	9	0,00098	6,8	0,000189	17	0,02	0,00	0,00072	3,0	14,26	0,42
	n5252mnzDuth3-20	302	28904	96	5	0,00137	5,7	0,000260	15	0,03	0,00	0,00065	3,0	12,73	0,38
	n5252mnzDuth3-21	462	35109	76	8	0,00108	7,6	0,000205	14	0,03	0,00	0,00069	3,0	13,51	0,40
DUTH6															
Group A	n5251mnzDuth6-01	118	21274	180	3	0,00151	5,6	0,000381	12	0,03	0,00	0,00064	3,0	12,60	0,37
	n5251mnzDuth6-02	138	17218	124	2	0,00143	7,4	0,000194	24	0,04	0,00	0,00060	3,1	11,71	0,35
	n5251mnzDuth6-03	130	15794	122	2	0,00156	9,3	0,000207	25	0,04	0,01	0,00061	3,2	11,81	0,36
	n5251mnzDuth6-07	183	17309	95	2	0,00192	6,3	0,000288	17	0,05	0,01	0,00061	3,0	11,66	0,34
	n5251mnzDuth6-12	164	17218	105	2	0,00180	6,7	0,000292	17	0,05	0,01	0,00060	3,0	11,59	0,34
	n5251mnzDuth6-13	198	19667	99	3	0,00132	7,7	0,000228	21	0,03	0,00	0,00057	3,1	11,14	0,33
	n5251mnzDuth6-17	101	20764	206	1	0,00191	7,5	0,000229	20	0,06	0,01	0,00061	3,0	11,58	0,34
	n5251mnzDuth6-18	112	20749	185	2	0,00176	8,7	0,000100	31	0,06	0,01	0,00066	3,0	12,49	0,36
	n5251mnzDuth6-19	137	21615	158	2	0,00175	8,5	0,000152	27	0,06	0,01	0,00064	3,1	12,30	0,36
	n5251mnzDuth6-20	149	22525	152	2	0,00149	7,4	0,000183	24	0,04	0,00	0,00063	3,0	12,17	0,36
	n5251mnzDuth6-21	95	19813	209	1	0,00150	9,1	0,000156	35	0,05	0,01	0,00062	3,1	11,88	0,36
	n5251mnzDuth6-22	120	25983	217	3	0,00127	5,9	0,000289	18	0,03	0,00	0,00062	3,0	12,13	0,36
Group B	n5251mnzDuth6-04	472	37595	80	8	0,00068	17,2	0,000057	58	0,02	0,00	0,00049	3,6	9,60	0,34
	n5251mnzDuth6-05	347	32644	94	5	0,00080	13,4	0,000159	29	0,02	0,00	0,00047	3,6	9,39	0,33
	n5251mnzDuth6-08	208	22308	108	2	0,00135	8,4	0,000156	28	0,04	0,00	0,00049	3,2	9,50	0,29
	n5251mnzDuth6-09	279	30751	110	2	0,00131	7,9	0,000256	22	0,03	0,00	0,00049	3,1	9,59	0,29
	n5251mnzDuth6-10	156	23427	150	2	0,00132	10,0	0,000222	28	0,03	0,01	0,00051	3,1	9,86	0,30
	n5251mnzDuth6-11	157	21747	138	2	0,00145	10,0	0,000088	38	0,05	0,01	0,00052	3,2	9,95	0,31
	n5251mnzDuth6-14	375	34770	93	5	0,00067	13,3	0,000135	41	0,02	0,00	0,00047	3,5	9,33	0,32
	n5251mnzDuth6-15	350	33077	94	5	0,00077	12,0	0,000121	37	0,02	0,00	0,00052	3,2	10,20	0,32
	n5251mnzDuth6-16	452	47318	105	7	0,00071	14,1	0,000038	52	0,02	0,00	0,00047	3,4	9,33	0,31
	n5251mnzDuth6-23	188	33317	177	3	0,00111	6,9	0,000229	17	0,03	0,00	0,00051	3,0	10,08	0,30

Sample	Analysis ID	U ppm	Th ppm	Pb ppm	Th/U meas	$^{204}Pb/^{208}Pb$	$\pm\sigma$ %	$^{232}Th^{143}Nd^{16}O_2^{++}/^{208}Pb$	$\pm\sigma$ %	f208	$\pm\sigma$ %	$^{208}Pb/^{232}Th$ uncorr.	$\pm\sigma$ %	$^{208}Pb/^{232}Th$ Age corr. (Ma)	$\pm\sigma$ Ma
	n5251mnzDuth6-24	193	26741	139	3	0,00112	8,1	0,000353	16	0,02	0,00	0,00053	3,0	10,54	0,32
	n5251mnzDuth6-25	242	36400	150	4	0,00099	8,4	0,000092	28	0,03	0,00	0,00048	3,1	9,42	0,28
	n5251mnzDuth6-26	290	30574	105	4	0,00071	11,3	0,000190	25	0,01	0,00	0,00049	3,2	9,85	0,31
Unaligned	n5251mnzDuth6-06	687	33867	49	15	0,00042	22,8	b.d.	b.d.	0,02	0,00	0,00062	3,8	12,42	0,47
GRAESER1															
Group A	n4196-Graeser1@02	158	22871	145	17,3	0,00420	5,2	0,000219	25	0,15	0,01	0,00061	2,5	10,47	0,24
	n4196-Graeser1@03	175	24431	140	19,4	0,00376	6,4	0,000235	30	0,13	0,01	0,00056	2,6	9,80	0,24
	n4196-Graeser1@04	185	22202	120	20,0	0,00387	4,5	0,000192	20	0,14	0,01	0,00069	2,5	12,13	0,27
	n4196-Graeser1@05	173	23602	137	21,5	0,00334	8,0	0,000131	32	0,12	0,01	0,00055	2,6	9,80	0,24
	n4196-Graeser1@07	191	21452	112	20,0	0,00549	5,2	0,000288	22	0,19	0,01	0,00071	2,5	11,69	0,27
Group B	n4196-Graeser1@09	84	45075	534	20,2	0,00071	10,4	0,000205	21	0,01	0,00	0,00039	2,6	7,81	0,20
	n4196-Graeser1@10	100	44882	451	27,2	0,00095	11,2	0,000311	19	0,01	0,00	0,00040	2,5	8,00	0,20
	n4196-Graeser1@11	132	44210	334	26,2	0,00069	13,2	0,000126	32	0,02	0,00	0,00038	2,5	7,57	0,19
	n4196-Graeser1@12	139	42695	306	23,7	0,00088	11,6	0,000138	29	0,02	0,00	0,00039	2,5	7,60	0,19
	n4196-Graeser1@13	150	43561	291	24,4	0,00077	13,9	0,000295	27	0,01	0,01	0,00039	2,5	7,74	0,20
	n4196-Graeser1@14	140	42430	303	26,0	0,00081	11,4	0,000152	27	0,02	0,00	0,00039	2,5	7,69	0,19
Group C	n4196-Graeser1@15	74	37677	511	20,2	0,00177	5,8	0,000460	12	0,03	0,00	0,00059	2,6	11,43	0,29
	n4196-Graeser1@16	88	36126	409	24,3	0,00169	5,9	0,000340	15	0,04	0,00	0,00063	2,5	12,14	0,30
	n4196-Graeser1@20	106	45472	430	34,6	0,00137	7,9	0,000193	23	0,04	0,00	0,00054	2,5	10,54	0,26
	n4196-Graeser1@21	69	37655	548	19,7	0,00157	5,8	0,000362	14	0,03	0,00	0,00060	2,5	11,81	0,29
Group D	n4196-Graeser1@17	179	37755	211	62,2	0,00112	11,2	0,000082	42	0,04	0,00	0,00047	2,7	9,16	0,25
	n4196-Graeser1@18	136	43057	317	40,3	0,00122	9,9	0,000162	30	0,03	0,01	0,00048	2,7	9,31	0,25
	n4196-Graeser1@19	252	46797	186	44,4	0,00103	9,2	0,000072	33	0,03	0,00	0,00046	2,7	9,07	0,24
	n4196-Graeser1@29	180	42387	236	35,9	0,00145	8,0	0,000156	25	0,04	0,00	0,00047	2,6	9,10	0,23
Group E	n4196-Graeser1@22	74	31194	421	15,8	0,00214	9,1	0,000219	31	0,07	0,01	0,00049	2,5	9,26	0,23
	n4196-Graeser1@23	103	32802	317	24,5	0,00172	9,4	0,000147	35	0,06	0,01	0,00044	2,5	8,43	0,21
	n4196-Graeser1@24	108	33377	310	29,3	0,00179	8,9	0,000000	45	0,07	0,01	0,00045	2,6	8,47	0,21
	n4196-Graeser1@25	84	32877	393	24,8	0,00189	8,0	0,000132	33	0,06	0,01	0,00046	2,5	8,70	0,21
	n4196-Graeser1@26	92	38302	417	30,2	0,00153	9,7	0,000175	29	0,05	0,01	0,00046	2,6	8,81	0,22
	n4196-Graeser1@27	95	38612	405	28,6	0,00151	8,6	0,000131	31	0,05	0,01	0,00047	2,6	9,02	0,23
	n4196-Graeser1@28	106	37240	351	37,0	0,00156	8,8	0,000154	32	0,05	0,01	0,00046	2,6	8,84	0,22
Unaligned	n4196-Graeser1@1	117	51071	437	34,0	0,00389	5,7	0,000274	20	0,13	0,01	0,00069	2,5	12,13	0,28
	n4196-Graeser1@06	422	30334	72	45,4	0,00535	4,3	0,000249	21	0,19	0,01	0,00065	2,5	10,60	0,23
	n4196-Graeser1@08	180	22088	123	22,1	0,00119	6,7	0,000350	17	0,02	0,00	0,00045	2,5	8,90	0,22
	n4196-Graeser1@30	95	61055	641	35,0	0,00126	6,4	0,000346	13	0,02	0,00	0,00051	2,5	10,09	0,25
	n4196-Graeser1@31	61	48115	792	22,0	0,00120	7,1	0,000354	15	0,02	0,00	0,00048	2,5	9,56	0,24
GRAESER3															
Group A	n4194-Graeser3@03	29	3240	113	211,0	0,02219	4,4	b.d.	b.d.	0,86	0,04	0,00546	7,5	15,60	0,61
	n4194-Graeser3@04	10	2907	293	14,0	0,02103	6,3	b.d.	b.d.	0,81	0,05	0,00348	7,4	13,11	0,69
	n4194-Graeser3@05	10	2028	212	8,9	0,02159	7,3	b.d.	b.d.	0,84	0,06	0,00191	2,7	6,36	0,39
	n4194-Graeser3@06	11	2147	200	no data	0,02125	6,1	b.d.	b.d.	0,82	0,05	0,00315	2,7	11,34	0,57
	n4194-Graeser3@07	10	2385	243	12,4	0,00329	3,0	0,000217	12	0,11	0,00	0,00051	2,5	9,09	0,20
	n4194-Graeser3@08	9	2114	227	no data	0,00288	4,0	0,000198	16	0,10	0,00	0,00045	2,6	8,25	0,19
	n4194-Graeser3@09	9	1815	194	15,5	0,00314	3,4	0,000287	12	0,10	0,00	0,00058	2,5	10,58	0,24
Group B	n4194-Graeser3@02	286	85536	299	no data	0,01686	10,1	b.d.	b.d.	0,65	0,07	0,00149	2,5	10,47	0,69
	n4194-Graeser3@13	182	46919	258	30,3	0,00600	3,1	0,000203	18	0,22	0,01	0,00061	2,6	9,65	0,21
	n4194-Graeser3@14	371	94337	254	no data	0,00628	4,3	0,000129	28	0,23	0,01	0,00057	2,5	8,82	0,20
	n4194-Graeser3@15	295	77751	264	no data	0,00645	3,5	0,000160	26	0,24	0,01	0,00060	2,5	9,29	0,19
	n4194-Graeser3@16	388	75731	195	62,9	0,00684	2,5	0,000229	15	0,25	0,01	0,00058	2,5	8,81	0,18
	n4194-Graeser3@17	314	77921	248	no data	0,02547	2,0	b.d.	b.d.	0,99	0,02	0,03559	3,0	10,32	0,20
Group C	n4194-Graeser3@01	761	113623	149	49,7	0,01877	9,0	b.d.	b.d.	0,73	0,07	0,00175	2,5	9,68	0,64
	n4194-Graeser3@10	707	103778	147	49,0	0,00320	3,3	0,000241	13	0,11	0,00	0,00059	2,5	10,62	0,24
	n4194-Graeser3@11	665	97662	147	49,7	0,00831	2,9	0,000188	19	0,31	0,01	0,00062	2,5	8,64	0,17
	n4194-Graeser3@12	684	104060	152	49,3	0,00540	3,4	0,000198	20	0,19	0,01	0,00049	2,6	7,93	0,18

Sample	Analysis ID	U ppm	Th ppm	Pb ppm	Th/U meas	$^{204}Pb/^{208}Pb$	$\pm\sigma$ %	$^{232}Th^{143}Nd^{16}O_2^{++}/^{208}Pb$	$\pm\sigma$ %	f208	$\pm\sigma$ %	$^{208}Pb/^{232}Th$ uncorr.	$\pm\sigma$ %	$^{208}Pb/^{232}Th$ Age corr. (Ma)	$\pm\sigma$ Ma
GRAESER 4															
	n4193-Graeser4@01	106	1096	1.7	10.4	0,00572	14.3	0,000498	38	0,18	0,03	0,00074	3.2	12.25	0,51
	n4193-Graeser4@02	67	1071	1.4	16	0,00539	13.1	0,000602	38	0,16	0,03	0,00070	3.3	11.88	0.47
KLEM 1															
Group A	n5248mnzKlem1-01	252	31091	123	4,0	0,00173	5,8	0,000542	9	0,03	0,00	0,00054	2,5	10,64	0,26
	n5248mnzKlem1-02	314	35863	114	4,4	0,00160	6,3	0,000444	10	0,03	0,00	0,00048	2,5	9,42	0,23
	n5248mnzKlem1-17	158	24793	157	1,6	0,00345	7,8	0,000388	11	0,10	0,01	0,00058	2,6	10,45	0,27
	n5248mnzKlem1-18	229	30290	132	3,4	0,00149	6,0	0,000342	14	0,03	0,00	0,00050	2,5	9,77	0,24
	n5248mnzKlem1-19	194	25788	133	2,9	0,00141	11,2	0,000319	15	0,03	0,01	0,00048	2,6	9,48	0,25
	n5248mnzKlem1-25	257	26012	101	3,0	0,00186	5,0	0,000449	11	0,04	0,00	0,00049	2,6	9,56	0,24
Group B	n5248mnzKlem1-03	119	14813	125	1,8	0,00149	8,1	0,000414	19	0,03	0,01	0,00053	2,7	10,50	0,28
	n5248mnzKlem1-04	153	17432	114	2,1	0,00125	10,8	0,000478	17	0,01	0,01	0,00045	2,5	9,08	0,24
	n5248mnzKlem1-05	166	17053	103	2,2	0,00109	11,2	0,000305	24	0,02	0,01	0,00048	2,6	9,44	0,25
	n5248mnzKlem1-07	79	14327	182	0,6	0,00465	4,0	0,000426	14	0,15	0,01	0,00060	2,6	10,36	0,24
	n5248mnzKlem1-08	90	13094	145	1,3	0,00127	10,8	0,000191	28	0,03	0,01	0,00049	2,6	9,64	0,25
	n5248mnzKlem1-09	115	13822	120	1,5	0,00160	10,1	0,000290	25	0,04	0,01	0,00048	2,6	9,39	0,24
	n5248mnzKlem1-10	145	17144	118	1,8	0,00180	9,1	0,000340	23	0,04	0,01	0,00044	2,7	8,56	0,23
	n5248mnzKlem1-11	113	14964	133	1,5	0,00172	7,8	0,000423	17	0,03	0,01	0,00050	2,5	9,84	0,24
	n5248mnzKlem1-12	151	17969	119	1,4	0,00190	8,4	0,000445	19	0,04	0,01	0,00041	2,6	7,97	0,20
Group C	n5248mnzKlem1-06	330	20280	61	4,4	0,00066	25,8	0,000099	58	0,02	0,01	0,00041	3,0	8,16	0,25
	n5248mnzKlem1-14	366	16222	44	2,0	0,00184	10,9	0,000315	19	0,05	0,01	0,00043	2,9	8,26	0,24
	n5248mnzKlem1-22	436	22622	52	3,1	0,00152	7,7	0,000333	18	0,03	0,01	0,00043	2,6	8,35	0,21
	n5248mnzKlem1-23	393	23562	60	3,1	0,00171	6,8	0,000388	15	0,04	0,01	0,00044	2,6	8,57	0,22
	n5248mnzKlem1-24	350	24388	70	3,0	0,00176	6,3	0,000427	14	0,04	0,00	0,00045	2,5	8,70	0,21
Group D	n5248mnzKlem1-13	229	15474	67	2,1	0,00181	7,8	0,000409	14	0,04	0,01	0,00054	2,5	10,39	0,26
	n5248mnzKlem1-15	235	10803	46	1,3	0,00241	9,1	0,000401	22	0,06	0,01	0,00048	2,6	9,16	0,24
	n5248mnzKlem1-16	161	11027	68	1,3	0,00184	8,6	0,000484	16	0,03	0,01	0,00052	2,6	10,17	0,26
	n5248mnzKlem1-21	268	17663	66	2,3	0,00189	5,8	0,000474	12	0,04	0,00	0,00051	2,5	10,02	0,24
KLEM2															
Group A	n5247mnzKlem2-01	364	24190	66	3,2	0,00236	7,8	0,000248	19	0,07	0,01	0,00073	2,5	13,65	0,33
	n5247mnzKlem2-02	452	23947	53	4,1	0,00194	8,2	0,000189	20	0,06	0,01	0,00072	2,6	13,64	0,34
	n5247mnzKlem2-03	442	16753	38	2,3	0,00307	11,2	0,000188	38	0,10	0,01	0,00056	3,2	10,17	0,32
	n5247mnzKlem2-04	736	28948	39	4,5	0,00211	9,3	0,000084	38	0,08	0,01	0,00055	2,9	10,24	0,29
	n5247mnzKlem2-05	339	21719	64	2,7	0,00259	7,5	0,000109	33	0,09	0,01	0,00066	2,6	12,04	0,30
	n5247mnzKlem2-06	294	10608	36	1,7	0,00359	11,8	0,000226	27	0,12	0,02	0,00075	2,7	13,24	0,38
	n5247mnzKlem2-08	175	12495	72	1,1	0,00207	13,0	0,000281	23	0,06	0,01	0,00071	2,6	13,55	0,37
	n5247mnzKlem2-09	199	11182	56	1,2	0,00181	16,7	0,000077	58	0,06	0,01	0,00069	2,7	13,05	0,36
Group B	n5247mnzKlem2-07	333	8242	25	1,1	0,00544	16,8	b.d.	b.d.	0,21	0,04	0,00059	2,9	9,47	0,40
	n5247mnzKlem2-12	532	8447	16	1,6	0,00201	34,0	0,000305	45	0,05	0,03	0,00053	4,4	10,07	0,50
	n5247mnzKlem2-16	398	5694	14	1,2	0,00498	9,8	0,000164	58	0,18	0,02	0,00059	3,7	9,79	0,35
	n5247mnzKlem2-17	270	6778	25	1,0	0,00238	10,5	0,000145	42	0,08	0,01	0,00058	2,8	10,73	0,30
Group C	n5247mnzKlem2-10	210	4922	23	0,8	0,00500	17,7	0,000257	38	0,17	0,03	0,00073	3,2	12,14	0,53
	n5247mnzKlem2-11	260	5206	20	0,9	0,00454	11,8	0,000080	100	0,17	0,02	0,00068	3,6	11,45	0,42
	n5247mnzKlem2-13	265	6605	25	1,0	0,00355	11,7	0,000116	42	0,13	0,02	0,00067	2,7	11,80	0,34
	n5247mnzKlem2-14	253	6404	25	1,1	0,00150	14,2	0,000152	55	0,05	0,01	0,00059	2,8	11,40	0,32
	n5247mnzKlem2-15	236	5398	23	0,9	0,00266	12,0	0,000154	42	0,09	0,01	0,00066	2,8	12,09	0,34
KLEM3															
Group A	n5243mnzKlem3-01	523	15424	29	2,8	0,00150	7,9	0,000271	19	0,04	0,00	0,00065	3,4	12,60	0,41
	n5243mnzKlem3-02	713	17226	24	3,3	0,00152	8,5	0,000217	22	0,04	0,01	0,00062	3,4	11,95	0,39
	n5243mnzKlem3-06	317	11270	36	2,0	0,00125	9,7	0,000262	22	0,03	0,01	0,00064	3,4	12,51	0,42
	n5243mnzKlem3-07	451	6603	15	1,5	0,00092	15,9	0,000406	29	0,00	0,01	0,00062	3,8	12,48	0,47
	n5243mnzKlem3-10	469	9721	21	1,9	0,00174	10,1	0,000269	28	0,05	0,01	0,00066	3,5	12,66	0,43
	n5243mnzKlem3-15	589	6134	10	1,5	0,00184	14,4	0,000337	30	0,05	0,01	0,00067	3,5	12,96	0,46
Group B	n5243mnzKlem3-03	3337	15521	5	5,6	0,00121	13,0	0,000228	30	0,03	0,01	0,00057	3,5	11,10	0,38

Sample	Analysis ID	U ppm	Th ppm	Pb ppm	Th/U meas	$^{204}Pb/^{208}Pb$	±σ %	$^{232}Th^{143}Nd^{16}O_2^{++}/^{208}Pb$	±σ %	f208	±σ %	$^{208}Pb/^{232}Th$ uncorr.	±σ %	$^{208}Pb/^{232}Th$ Age corr. (Ma)	±σ Ma
	n5243mnzKlem3-04	2200	15844	7	4,5	0,00100	13,0	0,000246	30	0,02	0,01	0,00057	3,4	11,28	0,39
	n5243mnzKlem3-05	2923	23744	8	7,9	0,00052	24,3	b.d.	b.d.	0,02	0,00	0,00047	3,8	9,26	0,35
	n5243mnzKlem3-22	2389	8081	3	3,1	0,00090	24,3	b.d.	b.d.	0,03	0,01	0,00053	3,7	10,43	0,39
	n5243mnzKlem3-23	2903	9666	3	4,1	0,00456	12,3	b.d.	b.d.	0,18	0,02	0,00051	3,8	8,43	0,32
Group C	n5243mnzKlem3-08	585	6083	10	1,4	0,00117	18,3	0,000193	50	0,03	0,01	0,00055	3,7	10,81	0,40
	n5243mnzKlem3-09	565	11293	20	1,8	0,00072	23,6	0,000142	43	0,02	0,01	0,00046	3,6	9,21	0,34
	n5243mnzKlem3-11	670	8406	13	1,6	0,00241	14,3	0,000148	50	0,08	0,01	0,00055	3,5	10,15	0,36
	n5243mnzKlem3-12	672	16136	24	3,0	0,00236	9,3	0,000184	32	0,08	0,01	0,00056	3,4	10,51	0,35
	n5243mnzKlem3-13	665	7722	12	1,7	0,00158	16,5	0,000169	52	0,05	0,01	0,00051	3,7	9,84	0,36
	n5243mnzKlem3-14	540	5580	10	1,4	0,00182	17,2	b.d.	b.d.	0,07	0,01	0,00057	3,7	10,68	0,39
	n5243mnzKlem3-24	788	8097	10	1,9	0,00229	15,7	0,000081	67	0,08	0,01	0,00056	3,6	10,32	0,37
Group D	n5243mnzKlem3-16	1050	9297	9	2,4	0,00158	11,3	0,000127	35	0,05	0,01	0,00064	3,4	12,32	0,41
	n5243mnzKlem3-17	1283	9403	7	2,6	0,00155	12,8	0,000033	100	0,06	0,01	0,00060	3,5	11,51	0,39
	n5243mnzKlem3-18	1219	10217	8	2,7	0,00111	14,6	0,000423	24	0,01	0,01	0,00062	3,4	12,44	0,43
	n5243mnzKlem3-19	1392	7965	6	2,3	0,00157	16,2	0,000459	31	0,03	0,01	0,00057	3,5	11,21	0,40
	n5243mnzKlem3-20	1278	8778	7	2,5	0,00120	16,2	0,000340	27	0,02	0,01	0,00065	3,4	12,95	0,45
	n5243mnzKlem3-21	1471	8781	6	2,6	0,00140	13,5	0,000095	71	0,05	0,01	0,00061	3,5	11,81	0,40
LUCO1															
Group A	n5240mnzLuco1-01	193	31917	165	4,3	0,00147	4,6	0,000335	11	0,03	0,00	0,00073	1,8	14,27	0,25
	n5240mnzLuco1-11	234	20709	89	3,3	0,00155	6,7	0,000220	18	0,04	0,00	0,00072	1,9	13,93	0,26
	n5240mnzLuco1-12	177	21657	122	3,1	0,00122	7,1	0,000276	18	0,03	0,00	0,00073	1,8	14,30	0,26
	n5240mnzLuco1-16	219	34430	157	5,3	0,00107	5,0	0,000325	10	0,02	0,00	0,00073	2,0	14,58	0,28
	n5240mnzLuco1-21	148	21950	149	3,1	0,00111	6,3	0,000333	13	0,02	0,00	0,00071	1,8	14,15	0,25
Group B	n5240mnzLuco1-02	273	32789	120	4,4	0,00144	5,4	0,000245	15	0,04	0,00	0,00065	1,6	12,59	0,20
	n5240mnzLuco1-03	283	32381	115	4,6	0,00165	5,5	0,000161	23	0,05	0,00	0,00065	1,6	12,49	0,20
	n5240mnzLuco1-13	435	29293	67	4,3	0,00123	8,1	0,000102	32	0,04	0,00	0,00051	1,8	9,90	0,17
	n5240mnzLuco1-14	294	24608	84	3,8	0,00132	8,4	0,000220	22	0,03	0,00	0,00054	1,8	10,48	0,19
	n5240mnzLuco1-15	335	26176	78	4,5	0,00124	9,8	0,000186	26	0,03	0,01	0,00052	2,4	10,23	0,24
	n5240mnzLuco1-22	225	27656	123	3,7	0,00105	7,6	0,000149	20	0,03	0,00	0,00059	1,6	11,64	0,18
	n5240mnzLuco1-23	307	29566	96	4,9	0,00075	9,7	0,000210	20	0,01	0,00	0,00056	1,6	11,16	0,18
	n5240mnzLuco1-24	314	28330	90	4,7	0,00067	10,1	0,000164	22	0,01	0,00	0,00057	1,6	11,33	0,18
	n5240mnzLuco1-25	326	28676	88	5,0	0,00078	9,9	0,000103	30	0,02	0,00	0,00056	1,6	11,04	0,18
Group C	n5240mnzLuco1-06	345	41126	119	7,6	0,00106	4,6	0,000296	10	0,02	0,00	0,00074	2,0	14,74	0,30
	n5240mnzLuco1-07	411	41364	101	7,7	0,00100	5,9	0,000298	12	0,02	0,00	0,00067	1,8	13,36	0,24
	n5240mnzLuco1-17	307	39762	129	6,5	0,00100	5,7	0,000245	13	0,02	0,00	0,00066	1,7	13,07	0,21
	n5240mnzLuco1-18	309	40907	132	6,4	0,00087	7,6	0,000214	14	0,02	0,00	0,00061	1,5	12,11	0,18
	n5240mnzLuco1-19	285	39267	138	6,1	0,00097	7,7	0,000196	14	0,02	0,00	0,00062	1,5	12,26	0,19
	n5240mnzLuco1-20	391	39996	102	7,6	0,00102	8,3	0,000211	19	0,02	0,00	0,00066	1,7	13,01	0,22
Group D	n5240mnzLuco1-04	563	41853	74	8,7	0,00081	12,3	0,000083	28	0,02	0,00	0,00057	1,8	11,28	0,20
	n5240mnzLuco1-05	816	44328	54	10,4	0,00103	10,8	0,000045	58	0,04	0,00	0,00052	1,9	10,03	0,19
	n5240mnzLuco1-08	663	51423	78	10,3	0,00075	7,8	0,000152	17	0,02	0,00	0,00054	1,6	10,66	0,17
	n5240mnzLuco1-09	561	48305	86	9,8	0,00088	7,9	0,000186	16	0,02	0,00	0,00059	1,6	11,69	0,18
	n5240mnzLuco1-10	603	46038	76	9,7	0,00076	9,2	0,000163	22	0,02	0,00	0,00055	1,6	11,00	0,18
SALZ2															
Group A	n5531mnz_Salz2@01	152	19346	127	2	0,00089	7,8	0,000291	14	0,01	0,00	0,00058	2,6	11,49	0,30
	n5531mnz_Salz2@2	216	24641	114	4	0,00066	10,9	0,000152	24	0,01	0,00	0,00056	3,6	11,10	0,40
	n5531mnz_Salz2@3	236	24776	105	4	0,00071	10,7	0,000158	30	0,02	0,00	0,00056	3,9	11,10	0,42
	n5531mnz_Salz2@4	270	25940	96	4	0,00038	16,5	0,000095	32	0,01	0,00	0,00052	3,5	10,47	0,37
	n5531mnz_Salz2@05	418	25847	62	5	0,00047	19,6	b.d.	b.d.	0,02	0,00	0,00053	4,1	10,52	0,42
	n5531mnz_Salz2@6	343	17493	51	3	0,00064	16,4	0,000155	33	0,01	0,00	0,00053	3,7	10,51	0,39
	n5531mnz_Salz2@7	438	19057	44	4	0,00051	17,7	0,000232	31	0,00	0,00	0,00053	3,9	10,68	0,42
	n5531mnz_Salz2@13	440	25569	58	6	0,00076	12,1	0,000042	52	0,03	0,00	0,00060	3,9	11,79	0,45
	n5531mnz_Salz2@26	566	19852	35	4	0,00058	15,6	0,000127	39	0,01	0,00	0,00054	4,3	10,69	0,45
Group B	n5531mnz_Salz2@8	218	11649	53	2	0,00134	8,1	0,000338	19	0,03	0,00	0,00066	2,4	13,02	0,31
	n5531mnz_Salz2@9	280	16542	59	3	0,00114	11,6	0,000177	31	0,03	0,01	0,00064	2,9	12,50	0,36

Sample	Analysis ID	U ppm	Th ppm	Pb ppm	Th/U meas	$^{204}Pb/^{208}Pb$	±σ %	$^{232}Th^{143}Nd^{16}O_2^{++}/^{208}Pb$	±σ %	f208	±σ %	$^{208}Pb/^{232}Th$ uncorr.	±σ %	$^{208}Pb/^{232}Th$ Age corr. (Ma)	±σ Ma
	n5531mnz_Salz2@10	268	16310	61	3	0,00122	8,6	0,000196	24	0,03	0,00	0,00068	2,4	13,32	0,32
	n5531mnz_Salz2@11	225	18945	84	3	0,00177	7,4	0,000166	24	0,06	0,01	0,00071	2,5	13,51	0,33
	n5531mnz_Salz2@12	275	16814	61	3	0,00147	9,2	0,000087	46	0,05	0,01	0,00064	3,9	12,21	0,46
	n5531mnz_Salz2@14	183	11882	65	2	0,00139	8,9	0,000261	21	0,03	0,01	0,00062	2,4	12,12	0,29
	n5531mnz_Salz2@15	210	12330	59	2	0,00107	9,2	0,000268	20	0,02	0,00	0,00066	2,5	13,02	0,33
	n5531mnz_Salz2@16	213	13094	62	2	0,00094	10,8	0,000167	27	0,02	0,00	0,00066	2,4	13,06	0,31
	n5531mnz_Salz2@17	245	13848	56	3	0,00103	9,9	0,000133	31	0,03	0,00	0,00068	2,5	13,25	0,32
	n5531mnz_Salz2@18	226	15082	67	2	0,00137	8,0	0,000188	27	0,04	0,00	0,00064	2,4	12,36	0,29
	n5531mnz_Salz2@20	217	7586	35	1	0,00164	8,1	0,000272	22	0,04	0,01	0,00066	2,5	12,69	0,31
	n5531mnz_Salz2@21	236	9668	41	2	0,00145	8,6	0,000360	21	0,03	0,01	0,00068	2,4	13,33	0,32
	n5531mnz_Salz2@22	242	12071	50	2	0,00115	10,0	0,000261	24	0,02	0,01	0,00064	2,7	12,70	0,34
	n5531mnz_Salz2@23	197	11083	56	2	0,00110	8,3	0,000250	19	0,02	0,00	0,00067	2,4	13,24	0,31
	n5531mnz_Salz2@24	248	12459	50	2	0,00105	9,4	0,000203	24	0,03	0,00	0,00067	2,4	13,18	0,32
	n5531mnz_Salz2@25	187	15083	81	2	0,00112	7,3	0,000267	18	0,02	0,00	0,00067	2,3	13,18	0,30
	n5531mnz_Salz2@27	326	16214	50	4	0,00135	9,2	0,000175	26	0,04	0,01	0,00073	2,9	14,19	0,41
Unaligned	n5531mnz_Salz2@19	707	18680	26	7	0,00080	22,9	0,000089	58	0,02	0,01	0,00063	5,1	12,51	0,63
	n5531mnz_Salz2@28	656	24974	38	11	0,00052	17,7	0,000045	67	0,02	0,00	0,00072	5,2	14,28	0,74
SCHIESS1															
Group A	n4197-Schiess1@1	201	27947	139	14,8	0,00169	7,9	0,000520	22	0,03	0,01	0,00046	2,5	8,90	0,23
	n4197-Schiess1@2	250	28067	112	15,6	0,00149	6,7	0,000344	14	0,03	0,00	0,00050	2,5	9,76	0,25
	n4197-Schiess1@4	146	25331	173	18,7	0,00139	9,7	0,000392	20	0,02	0,01	0,00053	2,5	9,52	0,25
	n4197-Schiess1@5	258	27142	105	11,8	0,00104	15,1	0,000318	22	0,02	0,01	0,00042	2,5	8,20	0,21
	n4197-Schiess1@6	251	31731	126	16,4	0,00125	13,6	0,000302	20	0,03	0,01	0,00040	2,5	7,89	0,20
	n4197-Schiess1@7	245	34231	140	17,9	0,00079	17,2	0,000100	51	0,02	0,01	0,00039	2,5	7,58	0,19
	n4197-Schiess1@11	200	25572	128	11,5	0,00148	8,7	0,000486	19	0,02	0,01	0,00048	2,5	9,58	0,24
	n4197-Schiess1@18	162	24741	153	15,0	0,00174	11,3	0,000319	26	0,04	0,01	0,00045	2,5	8,71	0,22
Group B	n4197-Schiess1@14	123	21385	173	9,3	0,00196	7,9	0,000547	16	0,03	0,01	0,00047	2,6	9,16	0,23
	n4197-Schiess1@15	131	19635	150	10,0	0,00167	9,1	0,000430	21	0,03	0,01	0,00051	2,5	9,94	0,25
	n4197-Schiess1@16	139	20868	150	10,7	0,00146	9,4	0,000461	22	0,02	0,01	0,00050	2,5	9,89	0,25
	n4197-Schiess1@17	135	21486	160	10,2	0,00150	8,8	0,000233	22	0,04	0,01	0,00051	2,5	9,85	0,24
	n4197-Schiess1@19	108	13890	129	6,0	0,00225	10,2	0,000390	25	0,06	0,01	0,00050	2,8	9,58	0,27
	n4197-Schiess1@20	83	16302	196	7,1	0,00142	10,8	0,000520	21	0,02	0,01	0,00048	2,5	9,62	0,25
Group C	n4197-Schiess1@21	102	13545	133	6,1	0,00274	10,6	0,000366	32	0,08	0,01	0,00042	2,6	7,80	0,21
	n4197-Schiess1@22	120	10132	85	4,8	0,00178	18,8	0,000509	41	0,03	0,02	0,00042	2,7	8,26	0,25
	n4197-Schiess1@23	191	15370	81	11,9	0,00255	14,0	b.d.	b.d.	0,10	0,01	0,00037	2,6	6,78	0,18
	n4197-Schiess1@24	240	14040	58	29,5	0,00327	18,1	b.d.	b.d.	0,13	0,02	0,00041	2,5	7,19	0,23
	n4197-Schiess1@25	141	14404	102	6,2	0,00104	19,4	0,000312	32	0,02	0,01	0,00038	2,5	7,48	0,19
	n4197-Schiess1@26	246	19903	81	16,7	0,00048	32,5	0,000149	58	0,01	0,01	0,00034	2,6	6,80	0,18
	n4197-Schiess1@27	164	12572	77	15,4	0,00626	9,7	0,000226	38	0,22	0,02	0,00045	2,6	7,01	0,22
Group D	n4197-Schiess1@3	366	47950	131	39,8	0,00357	9,5	0,000460	18	0,10	0,01	0,00045	2,5	8,84	0,22
	n4197-Schiess1@8	362	30511	84	21,5	0,00048	30,2	0,000000	71	0,02	0,01	0,00035	2,5	6,90	0,18
	n4197-Schiess1@9	613	26374	43	47,0	0,00202	9,0	0,000612	13	0,03	0,01	0,00036	2,6	7,08	0,18
	n4197-Schiess1@10	536	30173	56	55,5	0,00044	31,2	0,000158	50	0,00	0,01	0,00038	2,5	7,55	0,19
	n4197-Schiess1@12	410	32871	80	30,3	0,00081	17,7	0,000103	52	0,02	0,01	0,00040	2,5	7,84	0,20
	n4197-Schiess1@13	572	34082	60	61,7	0,00050	30,8	b.d.	b.d.	0,02	0,01	0,00042	2,8	8,31	0,24
TAMB1															
Group A	n4843mnz(Tamb1)_@09	68	2407	35	3,4	0,00294	13,7	0,000198	58	0,10	0,02	0,00066	2,9	13,49	0,40
	n4843mnz(Tamb1)_@10	68	1667	24	4,4	0,00091	25,1	b.d.	b.d.	0,04	0,01	0,00063	4,1	12,75	0,57
	n4843mnz(Tamb1)_@11	46	2012	43		0,00012	100,0	0,000140	100	-0,01	0,01	0,00063	3,0	12,56	0,39
	n4843mnz(Tamb1)_@12	58	1901	33		0,00044	44,8	b.d.	b.d.	0,02	0,01	0,00071	2,9	13,24	0,46
	n4843mnz(Tamb1)_@13	39	1174	30	2,9	0,02249	3,8	b.d.	b.d.	0,87	0,03	0,00562	12,0	14,73	0,53
Group B	n4843mnz(Tamb1)_@04	46	2026	44		0,00031	44,8	b.d.	b.d.	0,01	0,01	0,00078	2,9	15,07	0,47
	n4843mnz(Tamb1)_@05	41	1452	35		0,00028	70,8	b.d.	b.d.	0,01	0,01	0,00119	2,7	14,97	0,47
	n4843mnz(Tamb1)_@06	46	2235	48	3,4	0,00032	57,8	0,000257	71	-0,01	0,01	0,00077	2,9	14,02	0,44
	n4843mnz(Tamb1)_@07	51	2434	48		0,01827	3,5	0,000024	100	0,71	0,02	0,00070	2,6	13,68	0,36

Sample	Analysis ID	U ppm	Th ppm	Pb ppm	Th/U meas	$^{204}Pb/^{208}Pb$	$\pm\sigma$ %	$^{232}Th^{143}Nd^{16}O_2^{++}/^{208}Pb$	$\pm\sigma$ %	f208	$\pm\sigma$ %	$^{208}Pb/^{232}Th$ uncorr.	$\pm\sigma$ %	$^{208}Pb/^{232}Th$ Age corr. (Ma)	$\pm\sigma$ Ma
Group C	n4843mnz(Tamb1)_@19	39	2580	66		0,00092	19,0	0,000080	71	0,03	0,01	0,00438	3,1	17,33	0,30
	n4843mnz(Tamb1)_@20	66	2521	38	3,4	0,02205	2,0	b.d.	b.d.	0,85	0,02	0,00096	2,8	15,04	0,45
	n4843mnz(Tamb1)_@21	65	2121	33		0,01877	3,0	0,000019	100	0,72	0,02	0,00092	2,5	17,99	0,47
	n4843mnz(Tamb1)_@22	77	2266	30		0,00140	17,8	0,000265	45	0,03	0,01	0,00090	2,6	17,68	0,46
	n4843mnz(Tamb1)_@23	88	1681	19		0,02092	2,0	0,000071	35	0,80	0,02	0,00087	3,0	17,10	0,52
Unaligned	n4843mnz(Tamb1)_@1	50	3298	66		0,00063	50,1	0,000381	71	0,00	0,02	0,00097	2,6	18,92	0,48
	n4843mnz(Tamb1)_@02	29	1893	65		0,02479	1,4	0,000011	71	0,96	0,01	0,00989	2,6	8,32	0,11
	n4843mnz(Tamb1)_@03	38	1527	41		0,00205	27,9	b.d.	b.d.	0,08	0,02	0,00641	12,1	19,02	0,47
	n4843mnz(Tamb1)_@08	67	2944	44		0,01003	6,8	0,000156	58	0,38	0,03	0,00333	18,0	18,48	1,00
	n4843mnz(Tamb1)_@14	54	2186	40		0,00607	8,7	0,000107	71	0,23	0,02	0,00207	11,5	12,32	0,52
	n4843mnz(Tamb1)_@15	42	2370	56		0,00133	22,5	0,000161	71	0,04	0,01	0,00063	2,6	12,65	0,34
	n4843mnz(Tamb1)_@16	32	1461	46	2,4	0,00062	37,9	0,000107	100	0,02	0,01	0,00062	2,5	12,55	0,34
	n4843mnz(Tamb1)_@17	20	1195	61		0,00082	31,7	0,000197	71	0,02	0,01	0,00078	3,5	15,50	0,56
	n4843mnz(Tamb1)_@18	18	1228	69		0,00078	25,1	0,000059	100	0,03	0,01	0,00083	3,1	16,44	0,54
	n4843mnz(Tamb1)_@24	143	2213	15		0,00110	14,5	0,000138	45	0,03	0,01	0,00070	2,8	13,88	0,39
VALS															
Group A	n5255mnzVals-01	238	2600	11	1	0,00567	10,7	0,000158	50	0,21	0,02	0,00090	3,3	14,46	0,51
	n5255mnzVals-02	318	3414	11	1	0,00402	8,4	0,000197	38	0,14	0,01	0,00089	3,2	15,38	0,47
	n5255mnzVals-03	269	3516	13	1	0,00463	8,2	0,000271	39	0,16	0,02	0,00083	3,5	14,18	0,47
	n5255mnzVals-04	221	2879	13	1	0,00439	7,9	0,000364	36	0,14	0,01	0,00084	3,4	14,57	0,48
	n5255mnzVals-05	206	2904	14	1	0,00472	11,3	0,000113	58	0,17	0,02	0,00087	3,6	14,56	0,53
	n5255mnzVals-06	236	2509	11	1	0,00430	12,5	0,000155	50	0,15	0,02	0,00088	3,4	15,04	0,54
Group B	n5255mnzVals-07	34	12292	358	1	0,00179	10,3	0,000146	26	0,06	0,01	0,00084	3,1	15,98	0,47
	n5255mnzVals-08	47	10924	232	1	0,00171	8,2	0,000196	27	0,05	0,01	0,00078	3,1	14,97	0,45
	n5255mnzVals-09	45	10168	224	1	0,00233	16,4	0,000294	28	0,07	0,02	0,00079	3,1	14,95	0,49
	n5255mnzVals-10	42	8328	199	1	0,00200	7,6	0,000281	23	0,06	0,01	0,00079	3,1	15,05	0,45
	n5255mnzVals-11	47	7378	158	1	0,00169	9,1	0,000231	33	0,05	0,01	0,00077	3,2	14,73	0,45
	n5255mnzVals-12	33	5848	179	1	0,00222	7,7	0,000217	29	0,07	0,01	0,00085	3,1	15,91	0,48
	n5255mnzVals-13	35	6893	196	1	0,00178	10,8	0,000274	27	0,05	0,01	0,00080	3,1	15,39	0,47
Group C	n5255mnzVals-15	35	1879	53	0	0,00566	12,6	0,000419	45	0,19	0,03	0,00076	3,7	12,46	0,52
	n5255mnzVals-16	89	3056	34	1	0,00397	22,7	b.d.	b.d.	0,15	0,03	0,00071	3,8	12,09	0,57
	n5255mnzVals-24	42	1422	34	0	0,00555	9,1	0,000239	50	0,20	0,02	0,00087	3,6	14,18	0,50
	n5255mnzVals-25	52	1534	30	0	0,00661	9,3	0,000323	42	0,23	0,02	0,00083	4,2	12,83	0,52
	n5255mnzVals-30	55	2371	43	0	0,00537	8,3	b.d.	b.d.	0,21	0,02	0,00080	3,4	12,84	0,41
	n5255mnzVals-31	87	3492	40	1	0,00341	10,3	0,000099	67	0,12	0,01	0,00069	3,8	12,26	0,44
	n5255mnzVals-33	136	3474	25	1	0,00320	12,2	0,000205	58	0,11	0,02	0,00069	3,9	12,51	0,48
Group D	n5255mnzVals-35	614	3897	6	1	0,00240	15,8	0,000110	52	0,08	0,01	0,00076	3,2	14,15	0,46
	n5255mnzVals-36	719	3038	4	1	0,00286	12,4	0,000156	58	0,10	0,01	0,00070	3,5	12,77	0,44
	n5255mnzVals-37	842	3305	4	2	0,00183	15,3	b.d.	b.d.	0,07	0,01	0,00075	3,5	14,16	0,48
	n5255mnzVals-38	698	3496	5	2	0,00202	13,7	0,000141	58	0,07	0,01	0,00076	3,3	14,36	0,47
Group E	n5255mnzVals-14	26	1732	67	0	0,00513	11,5	0,000068	100	0,19	0,02	0,00083	3,8	13,47	0,52
	n5255mnzVals-17	50	1770	36	no data	0,00995	10,6	b.d.	b.d.	0,39	0,04	0,00115	4,0	14,30	0,69
	n5255mnzVals-18	61	1712	28	0	0,00463	10,8	0,000109	67	0,17	0,02	0,00084	3,4	14,06	0,48
	n5255mnzVals-19	73	923	13	0	0,00527	15,1	b.d.	b.d.	0,20	0,03	0,00085	4,0	13,65	0,61
	n5255mnzVals-20	76	935	12	0	0,00457	18,4	b.d.	b.d.	0,18	0,03	0,00094	3,9	15,58	0,71
	n5255mnzVals-22	81	1401	17	0	0,00560	9,7	0,000371	41	0,19	0,02	0,00085	3,5	13,91	0,50
	n5255mnzVals-23	55	1237	23	0	0,00480	10,5	0,000349	44	0,16	0,02	0,00091	3,8	15,47	0,58
	n5255mnzVals-26	61	1742	29	0	0,00655	8,8	0,000226	50	0,24	0,02	0,00085	3,9	13,19	0,49
	n5255mnzVals-27	93	1978	21	1	0,00399	20,0	0,000179	58	0,14	0,03	0,00090	3,5	15,68	0,68
	n5255mnzVals-28	76	1795	23	1	0,00356	14,9	0,000109	100	0,13	0,02	0,00091	3,7	16,02	0,62
	n5255mnzVals-29	38	1768	47	0	0,00415	9,6	0,000159	52	0,15	0,02	0,00082	3,4	14,08	0,46
	n5255mnzVals-32	54	2481	46	1	0,00218	14,5	b.d.	b.d.	0,08	0,01	0,00081	3,5	15,00	0,51
	n5255mnzVals-34	238	2889	12	1	0,00238	9,5	0,000142	45	0,08	0,01	0,00082	3,3	15,13	0,47
	n5255mnzVals-39	100	2271	23	1	0,00463	9,9	0,000344	33	0,15	0,02	0,00085	3,5	14,54	0,50
	n5255mnzVals-40	98	2258	23	1	0,00478	11,7	0,000331	35	0,16	0,02	0,00088	3,7	14,93	0,57
	n5255mnzVals-41	92	1775	19	0	0,00481	10,9	0,000226	50	0,17	0,02	0,00083	3,5	14,01	0,50

Sample	Analysis ID	U ppm	Th ppm	Pb ppm	Th/U meas	$^{204}Pb/^{208}Pb$	$\pm\sigma$ %	$^{232}Th^{143}Nd^{16}O_2^{++}/^{208}Pb$	$\pm\sigma$ %	f208	$\pm\sigma$ %	$^{208}Pb/^{232}Th$ uncorr.	$\pm\sigma$ %	$^{208}Pb/^{232}Th$ Age corr. (Ma)	$\pm\sigma$ Ma
	n5255mnzVals-42	81	1266	16	0	0,00598	12,1	b.d.	b.d.	0,23	0,03	0,00095	3,5	14,73	0,57
	n5255mnzVals-43	78	1803	23	0	0,00430	10,1	0,000347	40	0,14	0,02	0,00095	3,8	16,43	0,61
	n5255mnzVals-44	79	1151	15	0	0,00651	17,0	0,000262	52	0,23	0,04	0,00094	3,6	14,60	0,75
VANI4															
Group A	Vani4_20160715_@4	80	1046	13	0,2	0,00214	25,8	0,001101	41	0,00	0,03	0,00046	34,5	9,27	0,43
	Vani4_20160715_@5	64	831	13	0,2	0,00580	15,5	b.d.	b.d.	0,22	0,03	0,00049	35,5	7,65	0,35
	Vani4_20160715_@6	34	577	17	0,1	0,00312	21,1	0,000412	58	0,09	0,03	0,00045	36,5	8,32	0,37
	Vani4_20160715_@15	82	3253	39	0,2	0,00210	20,6	0,000276	68	0,06	0,02	0,00042	44,5	7,98	0,36
	Vani4_20160715_@17	73	1647	22	0,2	0,00131	31,9	0,000511	58	0,01	0,02	0,00044	46,5	8,78	0,41
	Vani4_20160715_@18	102	1725	17	0,3	0,00206	23,1	0,001172	33	-0,01	0,02	0,00040	47,5	8,09	0,40
	Vani4_20160715_@19	40	720	18	0,1	0,00348	26,1	b.d.	b.d.	0,13	0,04	0,00050	48,5	8,74	0,54
	Vani4_20160715_@20	54	1072	20	0,2	0,00389	21,8	b.d.	b.d.	0,15	0,03	0,00040	49,5	6,89	0,37
	Vani4_20160715_@21	126	2630	21	0,3	0,00343	16,6	0,000260	67	0,11	0,02	0,00043	50,5	7,67	0,30
Group B	Vani4_20160715_@7	44	2034	46	0,2	0,00197	23,1	0,000402	58	0,05	0,02	0,00042	37,5	8,11	0,35
	Vani4_20160715_@8	41	1792	44	0,1	0,00938	12,3	0,000415	58	0,33	0,05	0,00057	38,5	7,70	0,39
	Vani4_20160715_@9	38	1343	36	0,2	0,00195	21,9	0,000105	100	0,07	0,02	0,00041	39,5	7,81	0,27
	Vani4_20160715_@10	40	2305	58	0,2	0,00216	17,5	0,000538	38	0,04	0,02	0,00042	40,5	8,18	0,27
	Vani4_20160715_@11	33	2496	75	0,2	0,00175	19,7	0,000488	38	0,03	0,02	0,00045	41,5	8,88	0,32
	Vani4_20160715_@12	42	3035	72	0,2	0,00398	15,8	0,000144	100	0,14	0,02	0,00043	42,5	7,46	0,28
	Vani4_20160715_@13	41	2168	53	0,2	0,00232	26,9	0,000244	100	0,07	0,03	0,00045	43,5	8,37	0,47
VANI5															
Group A	n5239mnzVani5-01	51	2196	43	0,2	0,00574	12,3	0,000352	52	0,20	0,03	0,00043	2,8	7,04	0,25
	n5239mnzVani5-02	65	2173	33	0,2	0,00461	16,2	0,000334	58	0,15	0,03	0,00042	3,3	7,19	0,29
	n5239mnzVani5-03	80	1854	23	0,3	0,00345	31,0	b.d.	b.d.	0,13	0,04	0,00038	4,2	6,63	0,37
	n5239mnzVani5-04	77	2070	27	0,3	0,00416	17,9	0,000518	58	0,12	0,03	0,00042	4,7	7,51	0,39
	n5239mnzVani5-05	67	3368	50	0,3	0,00364	16,3	0,000313	58	0,12	0,02	0,00040	2,7	7,14	0,24
	n5239mnzVani5-06	47	1610	34	0,2	0,00571	15,2	0,001023	35	0,14	0,04	0,00047	3,1	8,07	0,36
Group B	n5239mnzVani5-07	70	2507	36	0,2	0,00475	15,7	0,000280	67	0,16	0,03	0,00034	3,1	5,69	0,22
	n5239mnzVani5-08	155	2561	17	0,4	0,00220	35,6	0,001050	72	0,01	0,04	0,00032	4,5	6,33	0,39
	n5239mnzVani5-09	122	3321	27	0,4	0,00576	17,4	0,000534	58	0,18	0,04	0,00029	3,6	4,86	0,24
	n5239mnzVani5-19	97	2479	25	0,2	0,00486	23,3	0,000599	58	0,14	0,05	0,00031	3,6	5,34	0,29
	n5239mnzVani5-20	112	2792	25	0,3	0,00114	39,3	b.d.	b.d.	0,04	0,02	0,00030	3,6	5,79	0,22
Group C	n5239mnzVani5-11	163	3252	20	0,4	0,00339	12,4	0,000475	32	0,10	0,02	0,00041	2,7	7,45	0,22
	n5239mnzVani5-12	191	5008	26	0,6	0,00321	11,7	0,000671	27	0,07	0,02	0,00036	2,3	6,81	0,18
	n5239mnzVani5-13	400	5730	14	0,8	0,00110	35,2	b.d.	b.d.	0,04	0,01	0,00026	2,8	5,01	0,15
	n5239mnzVani5-14	332	6912	21	0,8	0,00168	16,5	0,000641	32	0,02	0,01	0,00030	3,0	5,93	0,19
	n5239mnzVani5-15	534	10803	20	1.7	0.01317	7.7	b.d.	b.d.	0.51	0.04	0.00027	3.3	2.69	0,11
Group D	n5239mnzVani5-10	106	8172	77	0,7	0,00218	18,3	0,000222	52	0,07	0,02	0,00028	2,7	5,27	0,16
	n5239mnzVani5-16	51	7567	149	0,5	0,00251	10,8	0,000553	27	0,06	0,01	0,00039	2,0	7,44	0,17
	n5239mnzVani5-17	73	7714	106	0,6	0,00133	16,3	0,000726	29	0,00	0,01	0,00032	2,1	6,48	0,16
	n5239mnzVani5-18	93	5882	63	0,5	0,00198	17,8	0,000501	38	0,04	0,02	0,00029	2,8	5,54	0,17
VANI6															
Group A	n5241mnzVani6-01	66	18941	287	3,2	0,00092	7,4	0,000225	16	0,02	0,00	0,00083	1,7	16,47	0,27
	n5241mnzVani6-02	69	17397	252	3,3	0,00093	8,3	0,000235	18	0,02	0,00	0,00078	1,5	15,44	0,24
	n5241mnzVani6-03	77	19682	257	3,6	0,00075	9,8	0,000247	21	0,01	0,00	0,00076	1,7	15,27	0,26
	n5241mnzVani6-04	86	23210	270	4,3	0,00066	9,4	0,000138	32	0,02	0,00	0,00076	1,6	15,21	0,25
	n5241mnzVani6-05	95	26312	276	5,5	0,00076	9,5	0,000183	18	0,02	0,00	0,00074	1,6	14,75	0,23
	n5241mnzVani6-20	73	18673	256	3,3	0,00084	8,1	0,000226	25	0,02	0,00	0,00080	1,9	15,96	0,31
	n5241mnzVani6-21	93	20429	220	4,0	0,00059	10,6	0,000180	21	0,01	0,00	0,00075	1,8	15,07	0,28
Group B	n5241mnzVani6-06	161	28046	175	6,7	0,00068	7,6	0,000230	14	0,01	0,00	0,00082	2,1	16,41	0,35
	n5241mnzVani6-07	212	27694	131	7,5	0,00048	10,6	0,000209	19	0,00	0,00	0,00073	1,7	14,71	0,26
	n5241mnzVani6-08	161	30524	189	6,8	0,00069	7,4	0,000227	17	0,01	0,00	0,00080	1,9	16,08	0,31
	n5241mnzVani6-09	206	28904	141	7,0	0,00036	12,6	0,000068	33	0,01	0,00	0,00070	1,7	14,07	0,23
	n5241mnzVani6-10	249	37643	151	10,0	0,00031	14,6	0,000122	24	0,00	0,00	0,00066	1,6	13,38	0,21

Sample	Analysis ID	U ppm	Th ppm	Pb ppm	Th/U meas	$^{204}Pb/^{208}Pb$	$\pm\sigma$ %	$^{232}Th^{143}Nd^{16}O_2^{++}/^{208}Pb$	$\pm\sigma$ %	f208	$\pm\sigma$ %	$^{208}Pb/^{232}Th$ uncorr.	$\pm\sigma$ %	$^{208}Pb/^{232}Th$ Age corr. (Ma)	$\pm\sigma$ Ma
Group C	n5241mnzVani6-11	170	43506	256	8,3	0,00081	5,3	0,000269	10	0,01	0,00	0,00073	1,5	14,66	0,22
	n5241mnzVani6-12	172	40474	235	8,3	0,00068	6,9	0,000196	12	0,01	0,00	0,00076	1,6	15,18	0,24
	n5241mnzVani6-13	207	44357	215	10,3	0,00058	6,6	0,000203	13	0,01	0,00	0,00074	1,5	14,90	0,22
	n5241mnzVani6-14	202	44315	219	10,4	0,00068	7,8	0,000190	13	0,01	0,00	0,00073	1,5	14,55	0,22
	n5241mnzVani6-15	230	45314	197	11,0	0,00048	8,8	0,000195	14	0,00	0,00	0,00070	1,6	14,15	0,22
Group D	n5241mnzVani6-16	59	24194	412	3,4	0,00100	6,0	0,000231	13	0,02	0,00	0,00085	1,9	16,80	0,31
	n5241mnzVani6-17	54	26294	491	2,5	0,00105	6,6	0,000187	15	0,03	0,00	0,00075	1,6	14,78	0,23
	n5241mnzVani6-18	67	24041	357	2,8	0,00092	7,4	0,000144	27	0,02	0,00	0,00073	1,6	14,47	0,22
	n5241mnzVani6-19	66	21515	327	2,5	0,00135	6,9	0,000190	25	0,04	0,00	0,00071	1,7	13,74	0,23
Group E	n5241mnzVani6-22	138	21421	155	4,7	0,00113	9,8	0,000092	39	0,04	0,00	0,00063	1,9	12,32	0,23
	n5241mnzVani6-23	119	19239	161	4,1	0,00056	14,5	0,000268	23	0,00	0,00	0,00062	1,8	12,53	0,23
	n5241mnzVani6-24	131	20006	153	3,7	0,00060	14,0	0,000062	56	0,02	0,00	0,00054	1,7	10,62	0,18

Table A1: Ion microprobe Th-Pb isotope ratios and ^{232}Th-^{208}Pb ages

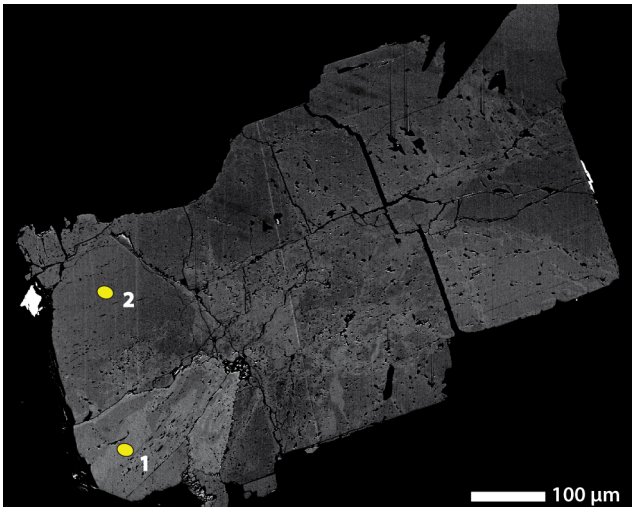

Figure A1. Backscatter electron image of monazite-(Nd) co-type material sample GRAESER 4 with the ovals representing the two measurement spots that yielded a Th-Pb age to scale.

Competing interests. No competing interests are present.

Acknowledgements. Fraukje Brouwer and Meinert Rahn are thanked for their detailed reviews that considerably improved this manuscript. We would also like to thank Anna Wenzel and Bernhard Grasemann for their editorial handling and helpful contact during manuscript revision. We greatly appreciate the help of M. Andres, R. Duthaler, M. Flepp, S. Graeser, L. Klemm, B. Hofmann, A. Salzmann, F. Vanini, and M. Walter by providing monazite-(Ce) samples for this study. This work was funded by the Swiss National Science Foundation, projects 200021-143972 and 200020-165513.

References

Aleinikoff, J.N., Schenk, W.S., Plank, M.O., Srogi, L., Fanning, C.M., Kamo, L. and Bosbyshell, H.: Deciphering igneous and metamorphic events in high-grade rocks of the Wilmington Complex, Delaware: Morphology, cathodoluminescence and backscattered electron zoning, and SHRIMP U-Pb geochronology of zircon and monazite. Geological Society of America Bulletin 118, 39-64, doi:10.1130/B25659.1, 2006.

Allaz, J., Engi, M., Berger, A. and Villa, I.M.: The effects of retrograde reactions and of diffusion on ^{40}Ar/^{39}Ar ages of micas. Journal of Petrology 52, 691-716, doi:10.1093/petrology/egq100, 2011.

Bergemann, C., Gnos, E., Berger, A., Whitehouse, M., Mullis, J., Pettke, T. and Janots, E.: Th-Pb ion probe dating of zoned hydrothermal monazite and its implications for repeated shear zone activity: An example from the central Alps, Switzerland. Tectonics 36, 671-689, doi:10.1002/2016TC004407, 2017.

Bergemann, C.A., Gnos, E., Berger, A., Whitehouse, M.J., Mullis, J., Walter, F. and Bojar, H.P.: Constraining long-term fault activity in the brittle domain through in-situ dating of hydrothermal monazite. Terra Nova 30, 440-446, doi:10.1111/ter.12360, 2018.

Bergemann, C.A., Gnos, E. and Whitehouse, M.J.: Insights into the tectonic history of the Western Alps through dating of fissure monazite in the Mont Blanc and Aiguilles Rouges massifs. Tectonophysics 750, 203-212, doi:10.1016/j.tecto.2018.11.013, 2019.

Berger, A., Gnos, E., Janots, E., Whitehouse, M.,Soom, M., Frei, R. and Waight, T.E.: Dating brittle tectonic movements with cleft monazite: Fluid-rock interaction and formation of REE minerals. Tectonics 32, 1-14, doi:10.1002/tect.20071, 2013.

Berger, A., Mercolli, I. and Engi, M.: The central Lepontine Alps: notes accompanying tectonic and petrographic map sheet Sopra Ceneri (1:100'000). Schweizerische mineralogische und petrographische Mitteilungen 85, 109-146, 2005.

Boston, K.R., Rubatto, D., Hermann, J., Engi, M. and Amelin, Y.: Geochronology of accessory allanite and monazite in the Barrovian metamorphic sequence of the Central Alps, Switzerland. Lithos 286-287, 502-518, doi:10.1016/j.lithos.2017.06.025, 2017.

Budzyn, B., Harlov, D.E., Williams, M.L. and Jercinovic, M.J.: Experimental determination of stability relations between monazite, fluorapatite, allanite, and REE-epidote as a function of pressure, temperature, and fluid composition. American Mineralogist 96, 1547-1567, doi:10.2138/am.2011.3741, 2011.

Campani, M., Mancktelow, N., Seward, D., Rolland, Y., Müller, W. and Guerra, I.: Geochronological evidence for continuous exhumation through the ductile-brittle transition along a crustal-scale low-angle normal fault: Simplon Fault Zone, central Alps. Tectonics 29, TC3002, doi:10.1029/2009TC002582, 2010.

Campani, M., Mancktelow, N. and Courrioux, G.: The 3D interplay between folding and faulting in a syn-orogenic extensional system: the Simplon Fault Zone in the Central Alps (Switzerland and Italy). Swiss Journal of Geosciences 107, 251-271, doi:10.2138/am.2013.4336, 2014.

Cherniak, D.J., Watson, E.B., Grove, M. and Harrison, T.M.:. Pb diffusion in monazite: A combined RBS/SIMS study. Geochimica et Cosmochimica Acta 68, 829-840, doi:10.1016/j.gca.2003.07.012, 2004.

Cherniak, D.J. and Pyle, J.M.: Th diffusion in monazite. Chemical Geology 256, 52-61, doi:10.1016/j.chemgeo.2008.07.024, 2008.

Dallmeyer, R.D., Neubauer, F., Handler, R., Fritz, H., Müller, W., Pana, D. and Putis, M.:Tectonothermal evolution of the internal Alps and Carpathians: Evidence from ^{40}Ar/^{39}Ar mineral and wholerock data. Eclogae geologicae Helvetiae, 89, 203–227, doi: 10.5169/seals-167900, 1996.

Elfert, S., Reiter, W. and Spiegel, C.: Long-lasting tectonic activities of the Lepontine Dome. New evidence from low-temperature thermochronology. Tectonophysics 608, 222-236, doi:10.1016/j.tecto.2013.09.033, 2013.

Fügenschuh, B., Mancktelow, N.S. and Seward, D.: Cretaceous to Neogene cooling and exhumation history of the OetztalStubai basement complex, eastern Alps: A structural and fission track study. Tectonics, 19, 905–918, doi:10.1029/2000TC900014, 2000.

Gasquet, D., Bertrand, J.-M., Paquette, J.-L., Lehmann, J., Ratzov, G., De Ascencao Guedes, R., Tiepolo, M., Boullier, A.-M., Scaillet, S. and Nomade, S.: Miocene to Messinian deformation and hydrothermal activity in a pre-Alpine basement massif of the French western Alps: new U-Th-Pb and Argon ages from the Lauzière massif. Bulletin de la Société Géologique de France 181, 227-241, doi:10.2113/gssgfbull.181.3.227, 2010.

Gnos, E., Janots, E., Berger, A., Whitehouse, M., Walter, F., Pettke, T. and Bergemann, C.:. Age of cleft monazites in the eastern Tauern Window: constraints on crystallization conditions of hydrothermal monazite. Swiss Journal of Geosciences 108, 55-74, doi:10.1007/s00015-015-0178-z, 2015.

Grand′Homme, A., Janots, E., Seydoux-Guillaume, A.-M., Guillaume, D., Bosse, V. and Magnin, V.: Partial resetting of the U-Th-Pb systems in experimentally altered monazite: Nanoscale evidence of incomplete replacement. Geology 44, 431-434, doi:10.1130/G37770.1, 2016.

Grand′Homme, A., Janots, E., Seydoux-Guillaume, A.-M., Guillaume, D., Magnin, V., Hövelmann, J, Höschen, C. and Boiron, M.C.: Mass transport and fractionation during monazite alteration by anisotropic replacement. Chemical Geology 484, 51-68, doi:10.1016/j.chemgeo.2017.10.008, 2018.

Grosjean, G., Sue, C. and Burkhard, M.: Late Neogene extension in the vicinity of the Simplon fault zone (central Alps, Switzerland). Eclogae Geologicae Helveticae 97, 33-46, doi:10.1007/s00015-004-1114-9, 2004.

Herwegh, M., Herwegh, M. and Pettke, T.: Titanium-in-quartz thermometry on synkinematic quartz veins in a retrograde crustal-scale normal fault zone. Tectonophysics 608, 468-481, doi:10.1016/j.tecto.2013.08.042, 2013.

Harrison, T.M., McKeegan, K.D. and LeFort, P.: Detection of inherited monazite in the Manaslu leucogranite by ion microprobe dating: crystallization age and tectonic implications. Earth and Planetary Science Letters 133, 271-282, doi:10.1016/0012-821X(95)00091-P, 1995.

Heijboer, T.C.: Origin and pathways of pro- and retrograde fluids, PTt paths and fluid-mineral equilibria from Alpine veins of the Central Alps: Case studies of the Fibbia and Amsteg areas. PhD thesis, University of Basel, Basel, Switzerland, doi:10.5451/unibas-004552692, 2006.

Herwartz, D., Nagel, T.J. Münker, C., Scherer, E.E. and Froitzheim, N.: Tracing two orogenic cycles in one eclogite sample by Lu-Hf garnet chronometry. Nature Geoscience 4, 178-183, 2011.

Hurford, A.J.: Cooling and uplift patterns in the Lepontine Alps, south-central Switzerland, and an age of vertical movement on the Insubric fault line. Contributions to Mineralogy and Petrology 93, 413-427, doi:10.1007/BF00374424, 1986.

Janots, E., Grand′Homme, A., Bernet, M. Guillaume, D., Gnos, E., Boiron, M.-C., Rossi, M., Seydoux-Guillaume, A.-M. and De Asencao Guedes, R: Geochronological and thermometric evidence of unusually hot fluids in an Alpine fissure of Lauziere granite (Belledonne, Western Alps). Solid Earth 10, 211-223, doi: 10.5194/se-10-211-2019, 2019.

Janots, E., Berger, A., Gnos, E., Whitehouse, M.J., Lewin, E. and Pettke, T.: Constraints on fluid evolution during metamorphism from U-Th-Pb systematics in Alpine hydrothermal monazite. Chemical Geology 326/327, 61-71, doi:10.1016/j.chemgeo.2012.07.014, 2012.

Janots, E., Engi, M., Rubatto, D., Berger, A., Gregory, C. and Rahn, M.: Metamorphic rates in collisional orogeny from in situ allanite and monazite dating. Geology 37, 11-14, doi:10.1130/G25192A.1, 2009.

Keller, L.M., Fügenschuh, B., Hess, M., Schneider, B. and Schmid, S.M.: Simplon fault zone in the western and central Alps: Mechanism of Neogene faulting and folding revisited. Geology 34, 317-320, doi:10.1130/G22256.1, 2006.

Keller, L.M., Hess, M., Fügenschuh, B. and Schmid, S.M.: Structural and metamorphic evolution of the Camughera-Moncucco, Antrona and Monte Rosa units southwest of the Simplon line, Western Alps. Eclogae Geologicae Helveticae 98, 19-49, doi:10.1007/s00015-005-1149-6, 2005.

Kirkland, C.L., Whitehouse, M.J. and Slagstad, T.: Fluid-assisted zircon and monazite growth within shear zones: a case study from Finnmark, Arctic Norway. Contributions to Mineralogy and Petrology 158, 637-657, doi:10.1007/s00410-009-0401-x, 2009.

Köppel, V. and Grünenfelder, M.: Concordant U-Pb ages of monazite and xenotime from the Central Alps and the timing of the high temperature Alpine metamorphism, a preliminary report. Schweizerische Mineralogische und Petrographische Mitteilungen 55, 129-132, 1975.

Kurz, W., Wölfler, A., Rabitsch, R. and Genser, J.: Polyphase movement on the Lavanttal Fault Zone (Eastern Alps): Reconciling the evidence from different geochronological indicators. Swiss Journal of Geosciences, 104, 323–343, doi:10.1007/s00015-011-0068-y, 2011.

Leu, W.: Lithostratigraphie und Tektonik der nordpenninischen Sedimente in der Region Bedretto-Baceno-Visp. Eclogae Geologicae Helvetiae 79, 769-824, 1986.

Ludwig, K.: Isoplot v.3.75: A Geochronological Toolkit for Microsoft Excel. Berkeley CA: Berkeley Geochronology Center Special Publication 5, 1-75, 2012.

Mancktelow, N.S.: Neogene lateral extension during convergence in the Central Alps: Evidence from interrrelated faulting and backfolding around the Simplonpass (Switzerland). Tectonophysics 215, 295-317, doi:10.1016/0040-1951(92)90358-D, 1992.

Markley, M.J., Teyssier, C., Cosca, M.A.,Caby, M.A., Hunsiker, J.C. and Sartori, M.: Alpine deformation and $^{40}Ar/^{39}Ar$ geochronology of synkinematic white mica in the Siviez-Mischabel Nappe, western Penninic Alps, Switzerland. Tectonics 17, 407-425, doi:10.1029/98TC00560, 1998.

Meldrum, A., Boatner, L.A. and Ewing, R.C.: A comparison of radiation effects in crystalline ABO(4)-type phosphates and silicates. Mineralogical Magazine, 64, 185-194, doi:10.1180/002646100549283, 2000.

Meldrum, A., Boatner, L.A., Wang, S.J., Wang, S.X. and Ewing, R.C.: Effects of dose rate and temperature on the crystalline-to-metamict transformation in the ABO(4) orthosilicates. Canadian Mineralogist, 37, 207-221, 1999.

Meldrum, A., Boatner, L.A., Weber, W.J. and Ewing, R.C.: Radiation damage in zircon and monazite. Geochimica et Cosmochimica Acta, 62, 2509-2520, doi:10.1016/S0016-7037(98)00174-4, 1998.

Meyre, C., Marquer, D. and Schmid, S.M.: Syn-orogenic extension along the Forcola fault: correlation of Alpine deformations in the Tambo and Adula Nappes (Eastern Penninic Alps). Eclogae Geologicae Helvetiae 91, 409-420, 1998.

Mullis, J.: P-T-t path of quartz formation in extensional veins of the Central Alps. Schweizerische Mineralogische und Petrographische Mitteilungen 76, 159-164, 1996.

Mullis, J., Dubessy, J., Poty, B. and O'Neil, J.: Fluid regimes during late stages of a continental collision: Physical, chemical, and stable isotope measurements of fluid inclusions in fissure quartz from a geotraverse through the Central Alps, Switzerland. Geochimica et Cosmochimica Acta 58, 2239-2267, doi:10.1016/0016-7037(94)90008-6, 1994.

Niggli, P., Königsberger, J. and Parker, R. L.: Die Mineralien der Schweizeralpen (661 pp.). Basel, B. Wepf & Co, 1940.

Parrish, R.R.: U-Pb dating of monazite and application to geological problems. Canadian Journal of Earth Sciences, 27, 1431–1450, doi:10.1139/e90-152, 1990.

Price, J.B., Wernicke, B.P., Cosca, M.A. and Farley, K.A.: Thermochronometry across the Austroalpine-Pennine boundary, Central Alps, Switzerland: Orogen-perpendicular normal fault slip on a major "overthrust" and its implications for orogenesis. Tectonics 37, 724-757, doi:10.1002/2017TC004619, 2018.

Purdy, J.W. and Stalder, H.A.: K-Ar ages of fissure minerals from the Schweizerische Mineralogische und Petrographische Mitteilungen 53, 79-98, 1973.

Putnis, A.: Mineral replacement reactions: From macroscopic observations to microscopic mechanisms. Mineralogical Magazine 66, 689-708, 2002.

Putnis, A.: Mineral replacement reactions. Reviews in Mineralogy and Geochemistry 70, 87-124, 2009.

Rahn, M.K.: Apatite fission track ages from the Adula nappe: late-stage exhumation and relief evolution. Schweizerische Mineralogische und Petrographische Mitteilungen 85, 233-245, doi:10.5169/seals-1662, 2005.

Ratschbacher, L., Frisch, W., Linzer, H.-G. and Merle O.: Lateral extrusion in the eastern Alps, Part 2: structural analysis. Tectonics 10, 257-271, doi:10.1029/90TC02623, 1991.

Ratschbacher, L., Frisch, W., Neubauer, F., Schmid, S.M. and Neugebauer J.: Extension in compressional orogenic belts: the eastern Alps. Geology 17, 404-407, doi:10.1130/0091-7613(1989)017<0404:EICOBT>2.3.CO;2, 1989.

Rauchenstein-Martinek, K.: Metamorphic fluid history along a cross section through the central Alps: constraints from LA-ICPMS analysis of fluid inclusions and Ar-Ar geochronology. PhD thesis. ETH Zürich, Zürich, 2014.

Regis, D., Rubatto, D., Darling, J., Cenki-Tok, B., Zucali, M. and Engi, M.: Multiple Metamorphic Stages within an Eclogite-facies Terrane (Sesia Zone, Western Alps) Revealed by Th–U–Pb Petrochronology. Journal of Petrology 55, 1429-1456, doi:10.1093/petrology/egu029, 2014.

Ricchi, E., Bergemann, C.A., Gnos, E., Berger, A., Rubatto, D. and Whitehouse, M.J.: Constraining deformation phases in the Aar Massif and the Gotthard Nappe (Switzerland) using Th-Pb crystallization ages of fissure monazite-(Ce). Lithos, in press, doi:10.1016/j.lithos.2019.04.014, 2019.

Rolland, Y., Cox, S., Boullier, A.M., Pennacchioni, G. and Mancktelow, N.:Rare earth and trace element mobility in mid-crustal shear zones: insights from the Mont Blanc Massif (Western Alps). Earth and Planetary Science Letters 214, 203-219, doi: 10.1016/S0012-821X(03)00372-8, 2003.

Rubatto, D., Gebauer, D. and Fanning, M.: Jurassic and Eocene subduction of the Zermatt-Saas-Fee ophiolites: implications for the geodynamic evolution of the Central and Western Alps. Contributions to Mineralogy and Petrology 158, 703-722, doi:10.1007/s004100050421, 1998.

Rubatto, D., Herrmann, J., Berger, A. and Engi, M.: Protracted fluid-induced melting during Barrovian metamorphism in the Central Alps. Contributions to Mineralogy and Petrology 158, 703-722, doi:10.1007/s00410-009-0406-5, 2009.

Ruffet, G., Gruau, G., Ballèvre, M., Féraud, G. and Phillipot, P.: Rb-Sr and ^{40}Ar-^{39}Ar laser probe dating of high-pressure phengites from the Sesia zone (Western Alps): underscoring of excess argon and new age constraints on the high-pressure metamorphism. Chemical Geology 141, 1-18, doi:10.1016/S0009-2541(97)00052-1, 1997.

Schärer, U., Cosca, M., Steck, A. and Hunziker, J.: Termination of major ductile strike-sli shear and differential cooling along the Insubric Line (Central Alps). Earth and Planetary Science Letters 142, 331-351, doi:10.1016/0012-821X(96)00104-5, 1996.

Schmid, S., Fügenschuh, B., Kissling, E., and Schuster, R.: The tectonic map and overall architecture of the Alpine orogen. Eclogae Geologicae Helveticae 97, 93-117, doi:10.1007/s00015-004-1113-x, 2004.

Seydoux-Guillaume, A.-M.,Montel, J.-M., Bingen, B., Bosse, V., de Parseval, P., Paquette, J.-L., Janots, E. and Wirth, R.: Low-temperature alteration of monazite: Fluid mediated coupled dissolution-precipitation, irradiation damage, and disturbance of the U-Pb and Th-Pb chronometers. Chemical Geology 330-331, 140-158, doi:10.1016/j.chemgeo.2012.07.031, 2012.

Sharp, Z.D., Masson, H. and Lucchini, R.: Stable isotope geochemistry and formation mechanisms of quartz veins; extreme paleoaltitudes of the Central Alps in the Neogene. American Journal of Science 305, 187-219, doi:10.2475/ajs.305.3.187 , 2005.

Stacey, J., Kramers, J.: Approximation of terrestrial lead isotope evolution by a two-stage model. Earth and Planetary Science Letters 26, 207-221, doi:10.1016/0012-821X(75)90088-6, 1975.

Steck, A., Della Torre, F., Keller, F., Pfeifer, H.-R., Hunziker, J. and Masson, H.: Tectonics of the Lepontine Alps: ductile thrusting and folding in the deepest tectonic levels of the Central Alps. Swiss Journal of Geociences 106, 427-450, doi:10.1007/s00015-013-0135-7, 2013.

Steck, A. and Hunziker, J.: The Tertiary structural and thermal evolution of the Central Alps-compressional and extensional structures in an orogenic belt. Tectonophysics 238, 229-254, doi:10.1016/0040-1951(94)90058-2, 1994.

Steiger, R.H., Jäger, E.: Subcommittee on Geochronology: Convention of the use of decay constants in geo- and cosmochronology. Earth and Planetary Science Letters 36, 359-362, doi:10.1016/0012-821X(77)90060-7, 1977.

Surace, I.R., Clauer, N., Thélin, P. and Pfeifer, H.-R.: Structural analysis, clay mineralogy and K-Ar dating of fault gouges from Centovalli Line (Central Alps) for reconstruction of their recent activity. Tectonophysics 510, 80-93, doi:10.1016/j.tecto.2011.06.019, 2011.

Townsend, K.J., Miller, C.F., D'Andrea, J.L., Ayers, J.C., Harrison, T.M. and Coath, C.D.: Low temperature replacement of monazite in the Ireteba granite, Southern Nevada: geochronological implications. Chemical Geology 172, 95-112, doi:10.1016/S0009-2541(00)00238-2, 2000.

Van Gelder, I. E., Willingshofer, E. and Andriessen, P. A. M.: Miocene to recent kinematics and exhumation of the Mur-Mürz strike-slip fault (Eastern Alps) illustrating direct interplay with surrounding lithospheric scale processes. Poster at the Alpine Workshop 2015, Briançon, France, 2015.

Wiederkehr, M., Bousquet, R., Schmid, S.M. and Berger, A.: From subduction to collision: thermal overprint of HP/LP meta-sediments in the north-eastern Lepontine Dome (Swiss Alps) and consequences regarding the tectono-metamorphic evolution of the Alpine orogenic wedge. Swiss Journal of Geosciences 101, 127-155, doi: 10.1007/s...15-008-1289-6, 2008.

Wiederkehr, M., Sudo, M., Bousquet, R., Berger, A. and Schmid, S.M.: Alpine orogenic evolution from subduction to collisional thermal overprint: The $^{40}Ar/^{39}Ar$ age constraints from the Valaisan Ocean, central Alps. Tectonics 28, 1-28, doi:10.1029/2009TC002496, 2009.

Zwingmann, H., and Mancktelow, N.: Timing of Alpine fault gouges. Earth and Planetary Science Letters 223, 415-425, doi:10.1016/j.epsl.2004.04.041, 2004.